Journal of Magnetic Resonance 280 (2017) 103–116

Contents lists available at ScienceDirect

Journal of Magnetic Resonance

journal homepage: www.elsevier.com/locate/jmr

Delocalisation of photoexcited triplet states probed by transient EPR and hyperfine spectroscopy

Sabine Richert [a,*], Claudia E. Tait [b,*], Christiane R. Timmel [a,*]

[a] Centre for Advanced Electron Spin Resonance (CAESR), Department of Chemistry, University of Oxford, South Parks Road, Oxford OX1 3QR, United Kingdom
[b] Department of Chemistry, University of Washington, Seattle, WA 98195, United States

ARTICLE INFO

Article history:
Received 11 December 2016
Revised 5 January 2017
Accepted 7 January 2017

Keywords:
Transient EPR
Triplet states
Delocalisation
Hyperfine techniques
ENDOR
Porphyrins
Molecular wires

ABSTRACT

Photoexcited triplet states play a crucial role in photochemical mechanisms: long known to be of paramount importance in the study of photosynthetic reaction centres, they have more recently also been shown to play a major role in a number of applications in the field of molecular electronics. Their characterisation is crucial for an improved understanding of these processes with a particular focus on the determination of the spatial distribution of the triplet state wavefunction providing information on charge and energy transfer efficiencies. Currently, active research in this field is mostly focussed on the investigation of materials for organic photovoltaics (OPVs) and organic light emitting diodes (OLEDs). As the properties of triplet states and their spatial extent are known to have a major impact on device performance, a detailed understanding of the factors governing triplet state delocalisation is at the basis of the further development and improvement of these devices. Electron Paramagnetic Resonance (EPR) has proven a valuable tool in the study of triplet state properties and both experimental methods as well as data analysis and interpretation techniques have continuously improved over the last few decades. In this review, we discuss the theoretical and practical aspects of the investigation of triplet states and triplet state delocalisation by transient continuous wave and pulse EPR and highlight the advantages and limitations of the presently available techniques and the current trends in the field. Application of EPR in the study of triplet state delocalisation is illustrated on the example of linear multi-porphyrin chains designed as molecular wires.

1. Introduction

The photoexcited triplet states of π-conjugated organic molecules designed for applications in solar energy conversion [1,2], molecular electronics [3] and spintronics [4] have received increased attention over the last two decades after initial focus on the properties of the corresponding singlet excitons. Methods for the characterisation of the properties of these triplet states, in particular the spatial extent of their wavefunctions in conjugated oligomers and polymers, are therefore of significant current interest. In systems designed as molecular wires, the extent of triplet state delocalisation provides information on the efficiency of electronic communication between the monomeric building blocks and understanding of the factors limiting triplet state delocalisation can guide the design of systems with improved charge transport properties. In materials for organic light emitting diodes (OLEDs) and organic photovoltaics (OPVs), the spatial extent of the excited triplet state was found to influence device performance significantly. For instance, spin-independent exciton recombination processes in fluorescence-based OLED devices should lead to generation of emissive singlet and non-emissive triplet excitons in a 1:3 ratio, limiting device performance to 25%. While this has indeed been observed for monomers, much higher percentages were encountered for conjugated polymers [5–8]. Enhanced delocalisation of the triplet state wavefunction was shown to prevent triplet recombination and favour processes such as triplet-triplet annihilation that recreate the emissive singlet state [2]. Detailed knowledge of the factors governing the extent of triplet state delocalisation is therefore of paramount importance in the optimisation of the photophysical processes in these devices.

Transient EPR spectroscopy is the technique of choice for the characterisation of the triplet state delocalisation, as the dark nature of the triplet states typically involved often prevents the application of any optical methods or makes such measurements very challenging. The extent of delocalisation may be estimated from the rates of triplet-triplet energy transfer, which depend on the

* Corresponding authors.
E-mail addresses: sabine.richert@chem.ox.ac.uk (S. Richert), cetait@uw.edu (C.E. Tait), christiane.timmel@chem.ox.ac.uk (C.R. Timmel).

http://dx.doi.org/10.1016/j.jmr.2017.01.005
1090-7807/

coupling strength between the triplets [9–11]. Highly localised states should exhibit a reduced coupling strength, but generally only rough estimates on the extent of triplet delocalisation are provided by such measurements. A better approach to access the delocalisation length of the excited triplet state involves the measurement of dielectric and magnetic susceptibilities. The dielectric polarisability volume is proportional to the polarisability per triplet molecule and contains information on the electrostatic confinement length scale of the excitons [12,13]. This approach has for example been used successfully to determine the extent of triplet delocalisation in substituted tetracene and pentacene derivatives [13]. However, compared to these methods, the information provided by measurement of the zero-field splitting (ZFS) parameters by EPR or optically detected magnetic resonance (ODMR) [14–16], or determination of the hyperfine coupling constants using Electron Nuclear DOuble Resonance (ENDOR) or Electron Spin Echo Envelope Modulation (ESEEM) techniques allows a much more precise quantification of the extent of triplet state delocalisation.

EPR spectroscopy has been widely applied to the investigation of triplet states involved in natural photosynthetic processes [21–32]. Triplet state delocalisation was investigated in the special pair (Fig. 1a) of bacterial and plant reaction centres by time-resolved EPR and triplet state ENDOR. The hyperfine coupling constants determined for the reaction centres using ENDOR were compared to those measured on the corresponding (bacterio)chlorophyll *a* monomers *in vitro*. In the reaction centres of *Rb. sphaeroides* and *Bl. viridis,* the triplet state was revealed to be unevenly delocalised over the two bacteriochlorophyll *a* units of the special pair [28,29,32]. On the other hand, the absence of changes in the hyperfine couplings in plant photosystem II, led to the conclusion that the triplet state is in this case localised on a single chlorophyll *a* unit of the special pair at cryogenic temperatures [27,31]. In photosystem I of cyanobacteria, comparison of the zero-field splitting parameters measured at room temperature and at cryogenic temperatures led to the proposal of delocalisation over both chlorophyll *a* molecules of the special pair at room temperature but localisation on a single unit at low temperatures [33]. The results on photosynthetic reaction centres indicated that the extent of triplet state delocalisation is very sensitive to the structural properties of the chlorophyll dimer and prompted further studies on a series of model porphyrin dimer systems (e.g. Fig. 1b) aimed at gaining more insight into the factors governing triplet state delocalisation in the special pair of different reaction centres [17,34]. While information from the comparison of the hyperfine interactions allowed precise determination of the extent of delocalisation of the excited triplet states in these studies, information from the ZFS parameters could not be unequivocally interpreted in terms of the extent of delocalisation.

Triplet state delocalisation in π-conjugated oligomeric structures designed for wire-like charge transport has also been investigated by EPR [18–20,35–38]. In these studies the determination of the extent of the triplet state wavefunction was based mainly on the interpretation of the zero-field splitting *D* value.

Analysis of the dependence of *D* on the first excited triplet state of thiophene oligomers (Fig. 1c) and interpretation of the experimental *D* values using calculations based on a π-electron model of the triplet wavefunction revealed localisation of the triplet excitation on about four thiophene rings [18,35].

A series of studies on different *meso*-to-*meso* ethynyl-linked zinc porphyrin oligomers (Fig. 1d) focussed on the interpretation of the ZFS *D* parameter determined by cw EPR in the framework of the point-dipole approximation [19,36,37]. The obtained average interelectron distances did not exceed the dimensions of a single monomeric porphyrin unit, which was interpreted in terms of spatially confined triplet states. This result was in contrast with results on the corresponding radical cations, where more extensive delocalisation was usually observed [39]. Based on a comparison of the $|E/D|$ ratio for different molecules, the authors proposed the occurrence of an oblate-to-prolate spin transition, *i.e.* a shift of the direction of maximum dipolar coupling in the molecular frame, for increased π-conjugation lengths [36,39,40]. A similar observation had been made before for stretched porphycenes [41].

More recent investigations on *meso*-to-*meso* butadiyne-bridged zinc porphyrin oligomers (Fig. 1e) combined time-resolved EPR for the determination of the zero-field splitting parameters and triplet state ENDOR and ESEEM for the characterisation of proton and nitrogen hyperfine couplings with DFT calculations to investigate triplet state delocalisation. Complete delocalisation of the triplet excited state over two porphyrin units was shown to occur in the dimer, while the triplet states were found to be unevenly delocalised with increased contribution of spin density on the central porphyrin units for longer oligomers [20,38]. Magnetophotoselection and orientation-selective ENDOR measurements provided experimental proof for the shift of the axis of maximum dipolar coupling from the out-of-plane axis in the porphyrin monomer to the long axis of the molecule in the oligomers. The observed changes in ZFS could be rationalised by comparison with the results of DFT calculations.

Excitation-wavelength dependent EPR measurements were used to analyse the influence of the dihedral angle between the porphyrin planes in porphyrin oligomers on the extent of triplet state delocalisation and showed localisation of the triplet state on a single porphyrin unit for conformers with perpendicular arrangements of adjacent porphyrin units [42]. On the other hand, no increase in delocalisation was observed for porphyrin ladders,

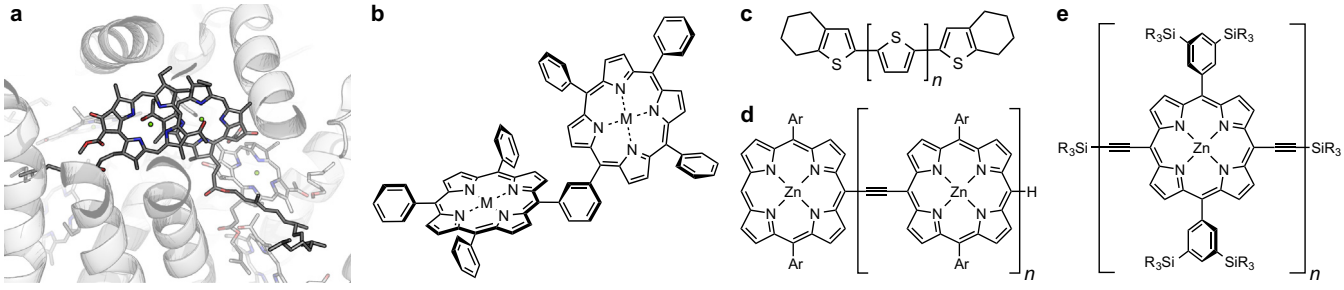

Fig. 1. Representative selection of chemical structures investigated in studies on triplet state delocalisation by EPR: special pair of the photosynthetic reaction centre of *Rb. sphaeroides* (4RCR.pdb) (**a**), porphyrin dimer (M = 2H, Zn) designed to investigate the influence of the relative arrangement of porphyrin units on energy and electron transfer processes [17] (**b**), oligothiophenes ($n \in \mathbb{N}_0$) [18] (**c**), meso-to-meso ethynyl-bridged zinc porphyrin oligomers ($n \in \mathbb{N}_0$, Ar = aryl substituent) [19](**d**), and *meso*-to-*meso* butadiyne-linked zinc porphyrin oligomers ($n \in \mathbb{N}$, R = hexyl) [20] (**e**) designed as molecular wires.

where adjacent porphyrin units are forced into an approximately coplanar arrangement [43].

In a study of triplet state delocalisation in a cyclic six-porphyrin nanoring, complete delocalisation over all six porphyrin units could be demonstrated by ^{1}H ENDOR [20]. The increased delocalisation compared to the corresponding linear system was attributed to the equivalence of the porphyrin units in the symmetric nanoring. This conclusion was further supported by a study revealing the importance of the electronic symmetry of the system for triplet state delocalisation [44].

In this paper, we review the currently available methods for the analysis of triplet state delocalisation by EPR and discuss their advantages and limitations. In Section 2, the practical aspects of EPR on photoexcited species are considered and the different experiments available for the characterisation of triplet states are presented. A theoretical background on EPR of triplet states is provided in Section 3 and the interpretation of triplet state EPR and hyperfine spectra is discussed with particular attention to the information they provide on the extent of triplet state delocalisation. In Section 4, the analysis of the spatial extent of the triplet state wavefunction by EPR is illustrated on the example of a series of linear zinc porphyrin oligomers. Finally, Section 5 summarises the current capabilities of EPR as a tool for the investigation of the extent of triplet state delocalisation, highlights current challenges and provides an outlook on future developments in this field.

2. Investigation of photoexcited triplet states by EPR

2.1. Generation of photoexcited species

The triplet states of the investigated molecules are typically generated by pulsed laser excitation of the sample inside the EPR resonator. In most cases, the excited triplet state is populated by intersystem crossing (ISC) from an excited singlet state. Under these conditions, the intensity of the observed triplet EPR signal is mainly dependent on (i) the quantum yield of triplet formation, (ii) the lifetime of the triplet state and the spin relaxation rates, (iii) the sample concentration, and (iv) the excitation wavelength and laser power used in the experiment. Experimentally, the sample concentration as well as the laser power can be optimised to maximise signal intensity. The parameters controlling the signal intensity which cannot (easily) be influenced are the quantum yield of triplet formation, the triplet lifetime and spin relaxation. Since the triplet lifetime can often be prolonged and spin relaxation considerably slowed down by performing the measurements under oxygen exclusion and at low temperatures, the feasibility of most triplet state experiments is determined by the quantum yield of triplet formation.

The excitation wavelength chosen for the experiments depends on the optical properties of the investigated samples. Frequently Nd:YAG lasers, operated at 532 nm and with a repetition rate of 10–20 Hz, have been used. Since this repetition rate often limits the shot repetition time of EPR experiments with laser excitation, the use of higher laser repetition rates may be advantageous (depending on the excited state lifetime and spin lattice relaxation). Typical laser pulse durations amount to 5–7 ns, implying that the time-resolution of the experiment is limited by the time-resolution of the spectrometer/detection. Depending on the triplet yield of the sample, excitation energies between 0.5 mJ and 10 mJ have normally been used. If tunability of the excitation wavelength is required in the experiment, Nd:YAG seeded optical parametric oscillators (OPOs) may be employed [42].

Excitation of the sample is achieved by guiding the laser light either directly through the optical window of the cryostat and resonator or, with the help of an optical fibre, through the top of the sample holder. Which one of the two options is preferred, depends on factors as diverse as the used resonator, spectrometer frequency, sample size, and the type of measurement to be performed. While for experiments at Q- and W-band, excitation through the top of the sample holder using an optical fibre may be preferable or even necessary, X-band measurements often profit from direct optical excitation through the optical window of the resonator. For measurements where excitation with polarised light is required, for instance, magnetophotoselection experiments, direct excitation is necessary. The linear polarisation of the laser light can easily be turned using a $\lambda/2$ waveplate. Alternatively, the excitation light can be depolarised using appropriate optical elements. For direct optical excitation, it is advisable to adapt the beam size and shape to the size of the optical window of the resonator and sample dimensions so as to maximise the illuminated sample area.

In a typical experiment, the sample is prepared at a concentration between 0.01 and 1 mM in a glass-forming solvent such as, for example, toluene or 2-methyltetrahydrofuran (MeTHF). Due to optical saturation effects (i.e. absorption of all the photons before the laser light reaches the back of the sample tube), high sample concentrations are not always advantageous. The optimal concentration can vary for different samples depending on their optical properties at the chosen excitation wavelength. Triplet state EPR experiments can also be performed in liquid crystals, where the alignment of the molecules can provide additional information on tensor orientations with respect to the molecular frame [45–47].

The EPR measurements are typically performed in solid matrices at low temperatures; the optimal temperature is determined by properties of the investigated system, the solvent used and the type of experiment to be performed. It is advantageous to perform pulse EPR experiments at temperatures where the spin lattice relaxation, determining the time-evolution of the triplet state sublevel populations, is slow and a high spin polarisation is maintained throughout the experiment. Moreover, other deactivation processes leading to the decay of the triplet state population, including molecular motion (e.g. tumbling, rotation of specific functional groups within the molecule), are also inhibited or much reduced at low temperatures.

2.2. TR-EPR

EPR spectra of transient paramagnetic species are typically recorded using a technique referred to as time-resolved EPR (TR-EPR) [48]. In this experiment, the EPR signal at a fixed magnetic field is recorded under continuous microwave (MW) irradiation as a function of time after the laser pulse generating the photoexcited state, see Fig. 2 (*left*). The magnetic field is stepped in order to obtain a 2D data set containing both spectral and temporal information as depicted in Fig. 2 (*left*). TR-EPR is performed without field modulation, yielding absorption instead of derivative EPR spectra. Alternatively, the triplet state EPR spectrum can also be obtained using standard cw-EPR with lock-in detection under steady-state illumination conditions.

Most triplet state EPR studies have been carried out at X- or Q-band frequencies ($\sim$9.5 GHz and $\sim$35 GHz, respectively). At these frequencies, the shape of the EPR spectrum is typically dominated by the zero-field splitting (ZFS) interaction for the triplet states of organic molecules, and its width is determined by the ZFS parameter D. TR-EPR performed at high frequencies has been used to resolve the g-tensor anisotropy and characterise the relative orientations of the g- and ZFS tensors [49].

On a typical Bruker spectrometer, TR-EPR can be performed using two different detection modes: direct detection or transient

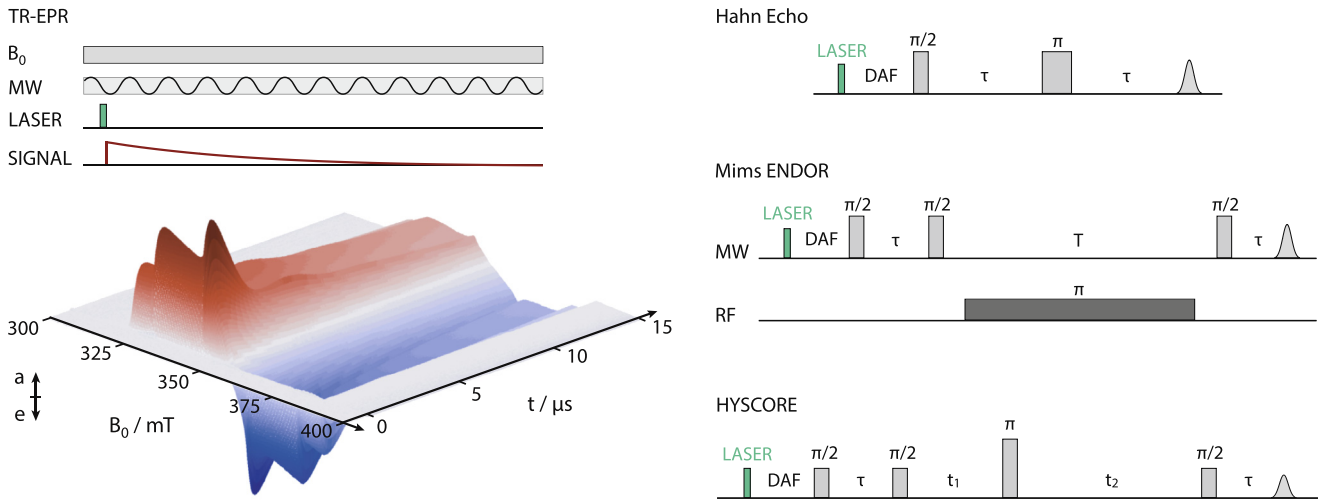

Fig. 2. Overview of the experimental transient EPR methods used for the investigation of triplet states. Time-resolved EPR (TR-EPR) sequence and example spectrum of a zinc porphyrin monomer (*left*) and examples of EPR pulse sequences referred to in the main text (*right*). MW: microwave; RF: radio frequency; DAF: delay after flash.

mode. In both cases, the measurement is carried out with a critically coupled resonator and the bandwidth of the resonator determines the response time. In order to measure fast responses, required for the detection of short-lived transient species, resonators with low Q-factors under matching conditions should be used. In a TR-EPR experiment with direct detection, the spectrometer is operated in cw mode and the digitiser is used to acquire the output of the preamplifier following the microwave diode detector [50]. The rise time of the transient signal and therefore the ability to detect short-lived species will be determined by the bandwidth of the preamplifier, in addition to the bandwidth of the resonator. In a TR-EPR experiment performed with the transient mode option of the spectrometer (see Bruker's Transient EPR User Guide for details), the signal from the resonator is downconverted by the IQ mixer, amplified by the video amplifier (bandwidth of 200 MHz) and digitised. In this mode, the microwave frequency must be locked using DC-AFC instead of AC-AFC. Both the in-phase and quadrature signals are acquired and the absorption EPR signal is typically obtained in the quadrature (imaginary) channel (assuming correct phasing during the tuning procedure). In both cases, the digitiser (SpecJet) needs to be triggered by the laser or by an external delay generator.

After data acquisition, baseline correction in both the time and field dimensions is performed to obtain the EPR spectrum as a function of time after the laser pulse. For this purpose, it is advisable to start acquisition about 500 ns before the laser pulse and use the initial points for background correction in the field dimension. The background correction in the time dimension is required to remove the laser background signal that can be recorded at an off resonance field position. For signal-to-noise improvements, the displayed transient EPR spectra are typically obtained by averaging over a certain time window, determined by the time-evolution characteristics of the signal.

2.3. Pulse EPR with laser excitation

In any pulse EPR experiment involving laser excitation, the laser or an external delay generator is used to trigger the spectrometer's pulse generator (PatternJet). The delay between the laser pulse, generating the photoexcited state, and the microwave pulse sequence is generally referred to as the delay after flash (DAF). This time interval is typically adjusted so as to maximise the EPR signal (depending on the evolution of the spin polarisation of the spectrum, the optimal value might differ for different field positions). The shot repetition time of pulse EPR experiments with laser excitation is typically determined by the shot-to-shot repetition rate of the laser.

Fig. 2 (*right*) shows three representative pulse EPR sequences for the study of triplet states. The laser excitation event and the DAF time delay are indicated in the figure. The two-pulse (Hahn echo) sequence can be used for the measurement of echo-detected field-swept EPR spectra. In the presence of significant nuclear modulation, undistorted EPR spectra can be obtained using FID-detection. Typically, triplet state EPR spectra recorded using pulse EPR show increased intensities at the canonical field positions and reduced signal intensities for non-canonical orientations compared to the corresponding spectra measured using TR-EPR. These differences have been attributed to anisotropic spin-spin relaxation induced by fluctuations of the ZFS tensor axes orientations [31,51]. Since the angular dependence of the ZFS interaction is stronger for non-canonical (off-axis) orientations, T_2 is shorter and the echo intensity is reduced compared to canonical orientations. In hyperfine spectra recorded at the canonical field positions, this effect also leads to enhanced contributions of the components of the hyperfine tensor aligned with the corresponding ZFS tensor axis [31].

Triplet state kinetics can be investigated by measurement of the two-pulse echo intensity as a function of the delay after the laser pulse [18,52,53].

The hyperfine interactions with different nuclei can be probed using ENDOR and/or ESEEM. As usual, the most suitable technique for a specific system depends on the magnitude of the couplings, the nuclei to be probed and the available spectrometer frequencies. For relatively large hyperfine couplings Davies ENDOR may be used [29,31,32], whereas Mims ENDOR is generally preferred for hyperfine couplings smaller than 5 MHz [20,38]. While triplet state ENDOR has so far mainly been used to probe proton couplings, triplet state ESEEM and HYSCORE [54] have been shown to be convenient methods for the measurement of deuterium and nitrogen hyperfine couplings [24,38,55,56].

In the presence of both stable and transient paramagnetic species, the contribution of the stable species in pulse EPR measurements can be selectively suppressed by preceding the laser pulse with a π inversion pulse and adjusting the delay between this pulse and the detection window of the pulse experiment to correspond to the zero-crossing point of the M_z magnetisation of the stable species [57], analogously to the REFINE (RElaxation FIltered hyperfiNE spectroscopy) method [58].

3. Triplet states in EPR

EPR on triplet states differs from EPR of spin $S = \frac{1}{2}$ systems in several important aspects, which will be illustrated in the following paragraphs.

3.1. Zero-field splitting interaction

The anisotropic magnetic dipole-dipole interaction between the two unpaired electrons in a triplet state leads to the removal of the degeneracy of the three triplet state sublevels even in the absence of an external magnetic field (see Fig. 3) and is referred to as the zero-field splitting (ZFS) interaction. The ZFS interaction is described by the Hamiltonian

$$\begin{aligned}\mathcal{H}_{\mathrm{ZFS}} &= \boldsymbol{SDS} = D_x S_x^2 + D_y S_y^2 + D_z S_z^2 \\ &= D\left(S_z^2 - \frac{1}{3}S^2\right) + E\left(S_x^2 - S_y^2\right)\end{aligned} \tag{1}$$

where D_x, D_y and D_z are the principal values of the ZFS tensor $\boldsymbol{D}$. Since the ZFS tensor is generally traceless, the ZFS interaction is typically specified using the two ZFS parameters D and E, defined as

$$D = \frac{3}{2}D_z \qquad E = \frac{1}{2}(D_x - D_y) \tag{2}$$

By convention, D and E are defined such that $|D| \geqslant 3|E|$ and $|D_z| \geqslant |D_x| \geqslant |D_y|$ [59], therefore the Z axis of the ZFS tensor corresponds to the axis of maximum dipolar coupling.

The energies of the triplet state sublevels at zero field, denoted as $|X\rangle, |Y\rangle$ and $|Z\rangle$ according to the axes of the ZFS tensor, $\boldsymbol{D}$, are given by

$$\begin{aligned}\mathcal{E}_X &= -D_x = \frac{1}{3}D - E \\ \mathcal{E}_Y &= -D_y = \frac{1}{3}D + E \\ \mathcal{E}_Z &= -D_z = -\frac{2}{3}D\end{aligned} \tag{3}$$

The energetic ordering of the zero-field triplet sublevels thus depends on the sign of D and E as shown in Fig. 3 for $D > 0, E < 0$ and $D < 0, E > 0$, respectively.

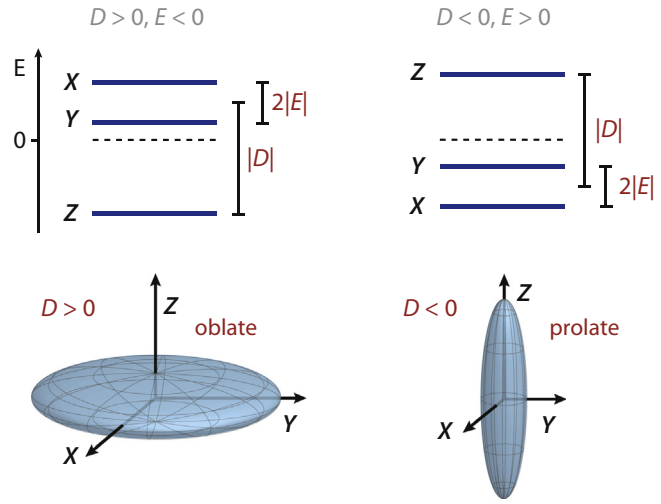

Fig. 3. Illustration of the zero-field splitting of the triplet energy levels in the absence of an external magnetic field and of the shape of the corresponding spin density distribution for $D > 0, E < 0$ (*left*) and $D < 0, E > 0$ (*right*). The energy differences between the triplet sublevels depend on the magnitudes of the zero-field splitting parameters $|D|$ and $|E|$ as indicated.

In most triplet states of organic compounds, the spin-orbit and crystal-field contributions to the ZFS interaction can be neglected and only the spin-spin contribution needs to be taken into account. The Hamiltonian can then be expressed in analogy to the classical dipole-dipole interaction and the ZFS parameters D and E can be formulated as

$$\begin{aligned}D &= \frac{3}{4}\frac{\mu_0}{4\pi h}(g_e\mu_B)^2\left\langle\frac{r^2 - 3z^2}{r^5}\right\rangle \\ &= \frac{3}{4}\frac{\mu_0}{4\pi h}(g_e\mu_B)^2\left\langle\frac{1 - 3\cos^2\theta}{r^3}\right\rangle\end{aligned} \tag{4}$$

$$E = \frac{3}{4}\frac{\mu_0}{4\pi h}(g_e\mu_B)^2\left\langle\frac{y^2 - x^2}{r^5}\right\rangle \tag{5}$$

where r is the distance between the unpaired electron spins, θ the angle between the spin-spin vector and the dipolar Z axis and the angular brackets indicate the expectation value. All other parameters have their usual meanings. From the above equations it can be seen that D can be related to the average inter-spin distance, whereas the parameter E contains information about the rhombicity of the ZFS tensor. For systems with axial symmetry $E = 0$, while $E \neq 0$ for systems with lower symmetry. The ratio $|E/D|$ is often specified and is a measure of the axiality of the ZFS tensor, where larger $|E|$ values indicate a strong non-axiality of the electron spin distribution.

The sign of D depends on the $(1 - 3\cos^2\theta)$ term of Eq. (4) and indicates whether the spin distribution is oblate ($D > 0$) or prolate ($D < 0$). Two extreme cases can be distinguished: For an oblate ('disk-like') spin distribution, θ can be considered equal to $\frac{\pi}{2}$, D is positive and the Z axis of maximum dipolar coupling is perpendicular to the plane of the spin distribution (molecular plane). For a prolate ('rod-like') spin distribution, θ can be considered equal to zero, giving a negative D and an axis of maximum dipolar coupling Z parallel to the long axis of the spin distribution (molecular axis) (cf. Fig. 3) [60].

Typically, the signs of the ZFS parameters D and E are not apparent from the triplet state EPR spectrum. The sign of D can be determined experimentally from the polarisation of triplet state EPR spectra measured at very low temperatures [61], by optically detected magnetic resonance (ODMR) [62] or by performing magnetophotoselection experiments [22,63,64]. Alternatively, the sign of D with respect to the sign of hyperfine couplings can be determined by hyperfine spectroscopy (see Section 3.3 for details) or predicted based on the molecular structure, for instance using DFT or other quantum chemical approaches. The sign of E, on the other hand, depends on the assignment of X and Y to the molecular axes and, following the convention for the definition of ZFS parameters mentioned above ($-1 \leqslant 3E/D \leqslant 0$ [59]) is chosen to be opposite to the sign of D.

3.2. The triplet state EPR spectrum

Triplet state EPR spectra are typically governed by the electronic Zeeman and zero-field splitting (ZFS) interactions. Since triplet state spectra are normally several hundred MHz wide, hyperfine coupling constants are only rarely resolved. In the presence of an external magnetic field, the energies of the triplet state sublevels are determined by both the zero-field splitting (ZFS) and the electronic Zeeman interactions. In the high-field approximation, the triplet spin states are typically denoted $|T_+\rangle, |T_0\rangle$ and $|T_-\rangle$, according to their energetic ordering in the high-field limit. These high-field spin states can be related to the zero-field spin states by mixing coefficients determined by the relative strengths of the Zeeman and ZFS interactions and the direction of the magnetic field [65]. If the external field B_0 is aligned with one of the principal axes of the ZFS tensor (canonical orientation), the energy

of the corresponding state is independent of B_0 and is equal to the energy at zero field, while the energies of the remaining two states increase and decrease, respectively, as a function of B_0 as shown in Fig. 4 (*top*). For example, for B_0 aligned with the Z axis, the energies of the triplet state sublevels are given by

$$\begin{aligned}\mathcal{E}_+ &= \frac{1}{3}D + \sqrt{E^2 + \left(\frac{g\mu_B}{h}B_0\right)^2}\\ \mathcal{E}_0 &= -\frac{2}{3}D\\ \mathcal{E}_- &= \frac{1}{3}D - \sqrt{E^2 + \left(\frac{g\mu_B}{h}B_0\right)^2}\end{aligned} \tag{6}$$

According to the selection rules in EPR, $\Delta m_S = \pm 1$, only transitions between the $|T_0\rangle$ level and the $|T_-\rangle$ or $|T_+\rangle$ levels are allowed. Depending on whether it corresponds to a $|T_0\rangle \leftrightarrow |T_+\rangle$ or $|T_0\rangle \leftrightarrow |T_-\rangle$ transition, the EPR transition will be denoted, for instance, Z^+ or Z^- in the case of $B_0 \parallel Z$. Based on the transition energies derived from Eq. (6), the distance between the magnetic fields corresponding to the low and high-field transitions for $B_0 \parallel Z, B_{hZ}$ and B_{lZ}, can be related to the magnitude of the ZFS parameter D [65]:

$$|2D| = \left(\frac{g\mu_B}{h}\right)^2 \frac{1}{2\nu}\left(B_{hZ}^2 - B_{lZ}^2\right) \approx \frac{g\mu_B}{h}\left(B_{hZ} - B_{lZ}\right) \tag{7}$$

Similarly, the distances between the two canonical transitions for $B_0 \parallel X$ and $B_0 \parallel Y$ can be related to $|D| + 3|E|$ and $|D| - 3|E|$, respectively. The canonical field positions are characterised by turning points in the powder or frozen solution EPR spectra of triplet states and can therefore be easily used to estimate $|D|$ and $|E|$ as shown in Fig. 4 (*bottom*). More precise values are obtained by numerical simulation of the spectrum.

In addition to the allowed $\Delta m_S = \pm 1$ transitions, the formally forbidden double-quantum ($\Delta m_S = \pm 2$) transitions at $g \sim 4$ can in some cases be observed for organic triplet states. Compared to the allowed transitions at $g \sim 2$, these transitions occur at half the field value and are therefore referred to as half-field transitions. Half-field transitions are generally narrower and weaker in intensity compared to the corresponding $\Delta m_S = \pm 1$ transitions and constitute a proof for the presence of a spin system with $S > \frac{1}{2}$ [66].

Photoexcited triplet states are typically generated with non-Boltzmann populations of the triplet sublevels due to selective population by ISC from the excited singlet state. Instead of an absorptive EPR spectrum, both absorptive and emissive transitions are therefore observed and the spectrum is referred to as being spin-polarised. The selective (over-)population of certain zero-field sublevels (*i.e.* spin polarisation) generally yields larger population differences between the states than would be observed in the case of Boltzmann populations, leading to enhanced signal intensities.

If the triplet is generated by ISC from the singlet state, the spin polarisation of the spectrum reflects selective population of the zero-field spin states. The populations of the high-field triplet state sublevels, $|T_{-1}\rangle, |T_0\rangle$, and $|T_{+1}\rangle$, which determine whether a particular transition is emissive or absorptive can then be calculated from the initial populations of the zero-field levels, $|X\rangle, |Y\rangle$, and $|Z\rangle$. In the high-field approximation the sublevel populations for $B_0 \parallel Z$ are for example given by

$$P_0 = P_Z \qquad P_{\pm 1} = \frac{1}{2}(P_X + P_Y) \tag{8}$$

and the intensity of the two transitions is then proportional to the population difference, $P_0 - P_{\pm 1}$. Analogous relationships hold for the remaining two canonical orientations. For each orientation of B_0, the low- and high-field lines therefore exhibit equal and opposite polarisations, *i.e.* one is absorptive and one is emissive. In many cases it can be instructive to analyse the particular electronic spin polarisation pattern observed for a certain species, since the sequence of absorptive (a) and emissive (e) transitions (for example *aaaeee* for the triplet state of a zinc porphyrin, **P1**) can in principle be related to the mechanism of triplet formation (see Section 4). The spin polarisation of the triplet spectrum is very sensitive even to small changes in the relative triplet state sublevel populations [67], which can therefore easily be extracted by simulation. Examples of spin-polarised spectra for different relative zero-field sublevel populations are shown in Fig. 5.

Triplet state formation by radical pair recombination leads to selective population of the high-field spin states and can yield the polarisation patterns *aeeaae* and *eaaeea* that cannot be obtained by ISC [26,67]. The *aeeaae* spin polarisation arises from selective population of the $|T_0\rangle$ state for each canonical orientation, while the *eaaeea* spin polarisation arises from overpopulation of the $|T_{\pm 1}\rangle$ states. An additional mechanism for triplet state forma-

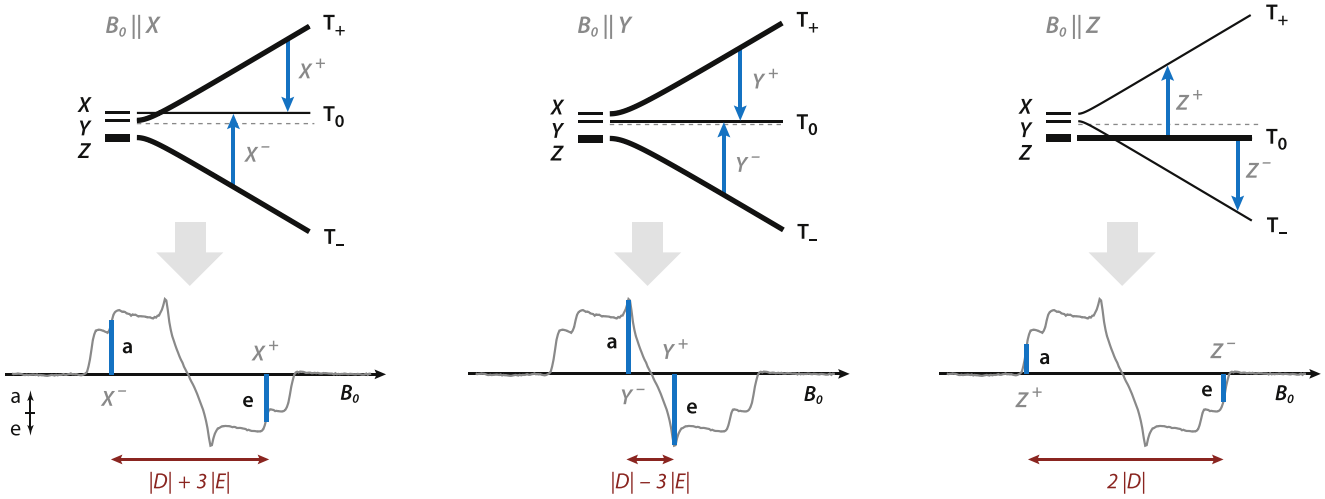

Fig. 4. Energies of the triplet sublevels of a triplet state with $D > 0$ and $E < 0$ as a function of an external magnetic field with the field vector, $\mathbf{B}_0$, aligned with the dipolar axes X, Y, and Z, respectively. Whenever the energy of the microwave radiation matches the energy gap between $|T_0\rangle$ and either $|T_-\rangle$ or $|T_+\rangle$, a transition can be observed. In a powder spectrum, the transitions corresponding to the canonical field orientations are characterised by turning points as illustrated by the spectrum shown for a zinc porphyrin monomer triplet state (Z zero-field sublevel primarily populated). The transitions can be either emissive (e) or absorptive (a) depending on the relative populations of the high-field sublevels involved, indicated by the thickness of the level bars.

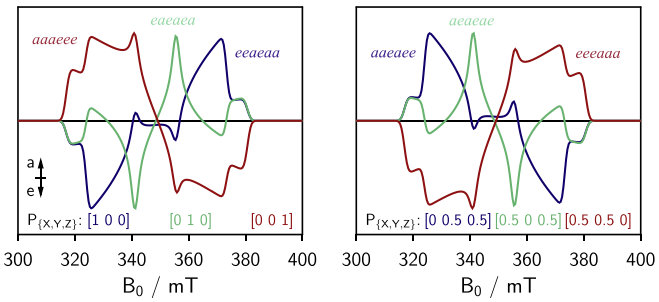

Fig. 5. Simulation of the triplet state EPR spectra ($D > 0$ and $E < 0$) for different relative populations of the triplet sublevels arising from selective population of the zero-field states *via* intersystem crossing.

tion is triplet-triplet energy transfer, where, due to conservation of the spin angular momentum, the spin polarisation of the acceptor triplet spectrum is determined by the spin polarisation of the donor triplet and the relative orientation of donor and acceptor [68–72].

3.3. Hyperfine spectroscopy for triplet states

Pulse EPR of triplet state systems is usually strongly orientation-selective, as typical microwave pulses of a couple of nanoseconds only excite a small fraction of the broad EPR spectrum (cf. Fig. 6). This leads to the contribution of only a limited number of orientations to the ENDOR or ESEEM spectra. In the most general case, $0 < |E| < |D|/3$, single-crystal-like spectra can be obtained for the Z field positions, while more orientations contribute at the X and Y field positions. If $|E| = |D|/3$, the X and Z transitions coincide and molecules with either of the corresponding ZFS tensor axes aligned with the magnetic field are excited, while orientation selection at Y is similar to the general case. For an axial ZFS tensor ($E = 0$), pure orientation selection is again obtained for the Z canonical transition, while orientations on the whole plane perpendicular to Z are excited for the remaining canonical transitions.

The ENDOR or ESEEM spectra recorded at different field positions therefore reflect the hyperfine couplings along the ZFS tensor orientations selected by the pulses [27,73]. If the hyperfine and ZFS tensors are collinear, measurements at the canonical field positions would yield the principal values of the hyperfine tensor directly. In a more general case, measurements performed at different field positions can allow determination of the relative orientation of the ZFS and hyperfine or quadrupole tensors. In practice, such an analysis can often be complicated by overlap of different canonical transitions or the presence of several coupled nuclei. Additional information, for example from quantum chemical modelling, can simplify the interpretation of the experimental data.

The additional transition selection present in pulse experiments on triplet states, *i.e.* selection of either the $m_S = 0 \leftrightarrow m_S = +1$ ($0 \leftrightarrow +1$) or the $m_S = -1 \leftrightarrow m_S = 0$ ($-1 \leftrightarrow 0$) transition, yields information on the relative sign of the hyperfine coupling with respect to the sign of the D value [27,73]. This is illustrated for ^{1}H ENDOR in Fig. 6. The energetic splittings and possible transitions for a triplet state coupled to a single $I = \frac{1}{2}$ nucleus in an external magnetic field, B_0, oriented along the ZFS Z axis are shown. The triplet state is assumed to be characterised by a positive D value ($D > 0$) and the hyperfine coupling along the Z axis of the ZFS tensor, A_Z, is also assumed to be positive and within the weak coupling regime ($0 < A_Z < \nu_I$). For each of the two triplet transitions, Z^+ and Z^-, the ENDOR spectra exhibit a peak at the nuclear Larmor frequency, arising from the nuclear transition frequency of the $m_S = 0$ manifold, and a peak arising from the other triplet manifold ($m_S = \pm 1$). As shown in Fig. 6, for the Z^+ transition, this peak is shifted by $-A_Z$ with respect to the Larmor frequency, while it is shifted by $+A_Z$ for the Z^- transition. For representation of the ENDOR spectra of weakly coupled nuclei such as ^{1}H, the Larmor frequency peak is generally set to zero, so that the x-axis directly reflects the magnitude of the hyperfine coupling constant in MHz. Since in most cases a series of orientations is selected and the hyperfine coupling is anisotropic, the ENDOR peaks corresponding to the $m_S = \pm 1$ manifolds are broadened by the distribution of hyperfine couplings, while the $m_S = 0$ peak, determined only by the nuclear Zeeman interaction [74,75], is typically much narrower.

The sign of the hyperfine coupling can be determined from the position of the ENDOR peak with respect to the Larmor frequency if the sign of the D value, and therefore the assignment of the low and high-field transitions to the + and − triplet transitions, is known. For $0 \leftrightarrow +1$ transitions, the hyperfine coupling constants associated with peaks located at frequencies lower than the Larmor peak are positive in sign, whereas those corresponding to peaks appearing at the higher frequency side of the Larmor peak are negative [73]. The opposite is true for $-1 \leftrightarrow 0$ transitions. A graphic summary of this is provided on the right in Fig. 6.

Similar considerations apply to ESEEM and HYSCORE experiments and for triplet states coupled to nuclei with $I > \frac{1}{2}$, where the presence of nuclear quadrupole interactions can cause a further

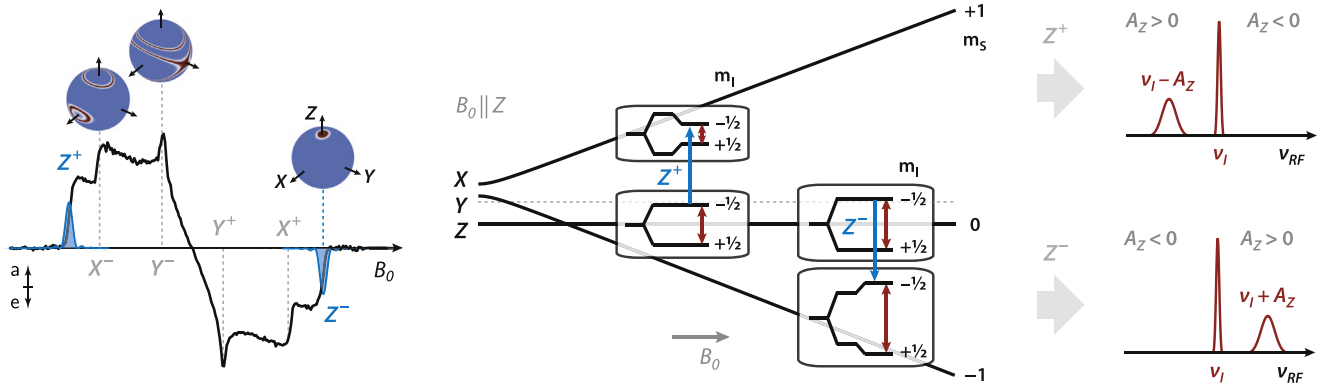

Fig. 6. Experimental zinc porphyrin triplet spectrum with unit spheres reflecting the orientation selection with a 16 ns microwave pulse applied at the canonical field positions (*left*). Schematic representation of the energy splittings for a triplet state coupled to an $I = \frac{1}{2}$ nucleus with $0 < A_Z < \nu_I$, $D > 0$, $E < 0$, and $B_0 \| Z$ (*centre*) and of the ENDOR spectra corresponding to the two EPR transitions (*right*). Allowed EPR transitions are shown in blue whereas nuclear transitions are indicated in red. The relative position of the observed ENDOR peak with respect to the Larmor peak is graphically illustrated. The position depends on the sign of the hyperfine coupling constant, A_Z, and the probed spin manifold. (For interpretation of the references to colour in this figure legend, the reader is referred to the web version of this article.)

splitting of the energy levels in all three manifolds. A particular feature of triplet state HYSCORE is the appearance of ridges parallel to the frequency axes if more than a single orientation is selected. This is due to the fact that the distribution of nuclear frequencies in the $m_S = \pm 1$ manifolds is larger than in the $m_S = 0$ manifold, as orientation-dependent changes in hyperfine couplings are usually more significant than changes in the nuclear Zeeman and nuclear quadrupole interactions [54].

One particular case that deserves attention is the cancellation regime ($A_i = \nu_I$) for a $I = 1$ nucleus such as ^{14}N. In this regime, not only the nuclear frequencies of the $m_S = 0$ manifold, but also the nuclear frequencies of one of the other manifolds do not depend on the hyperfine coupling and reduce to the pure nuclear quadrupole frequencies ($m_S = -1$ for $A_i < 0$ and $m_S = +1$ for $A_i > 0$). This implies that for one of the two triplet transitions no information on the hyperfine interaction is contained in the corresponding ESEEM or HYSCORE spectrum. The information on the hyperfine coupling is mainly contained in the double quantum peak of the spectrum corresponding to the other triplet transition. The sign of the hyperfine coupling can be determined from the relative positions of the double-quantum cross-peaks in the two triplet state transitions corresponding to each orientation. If the hyperfine coupling is positive, the larger nuclear frequencies are observed for the $-1 \leftrightarrow 0$ transition. If it is negative, the larger nuclear frequencies are observed for the $0 \leftrightarrow +1$ transition.

3.4. Triplet state delocalisation probed by EPR

Information on the extent of the triplet state wavefunction is contained in the ZFS and the hyperfine interactions. Triplet state delocalisation in oligomers and polymers can therefore be investigated by studying changes in the ZFS D parameter and the hyperfine couplings of different nuclei with respect to the monomeric unit. Triplet state delocalisation is in both cases probed on the timescale of the measured interaction; a static delocalisation cannot easily be distinguished from exciton hopping on a timescale faster than that characteristic of the probed interaction.

In the framework of the point-dipole approximation, the proportionality of the D value to $\langle r^{-3} \rangle$, where $\langle r \rangle$ is the average distance between the two unpaired electrons, can be exploited to determine the delocalisation length. It has, however, been shown that the use of the point-dipole approximation can lead to an underestimation of the inter-electron distance in the presence of significant delocalisation, as is the case for π-conjugated materials [76]. A further complication in the use of this approximation is the ambiguity in the definition of the principal ZFS axes; if the orientation of the ZFS tensor within the molecular framework and therefore the $(1 - 3\cos^2\theta)$ term in Eq. (4) changes with increasing oligomer length this needs to be taken into account for the correct interpretation of trends [38]. As an example, a change in spin distribution from an oblate ($\theta = 90°$) to an entirely prolate ($\theta = 0°$) system at a fixed average delocalisation length, $\langle r \rangle$, would result in an increase in the absolute value of D by a factor of two as seen from Eq. (4). In addition to excitation delocalisation (e.g. ^{3}**P2** for a dimer), a charge-transfer contribution to the ZFS (e.g. of the type $^3(\mathbf{P}^+\mathbf{P}^-)$) has also been identified in some porphyrin dimers and molecular complexes and has been shown to lead to a reduction in D compared to the single constituents [29,67,77,78]. Reliable quantification of the charge-transfer character in triplet states by EPR requires characterisation of the spin density distribution using hyperfine techniques [29].

An accurate interpretation of the ZFS interaction in terms of triplet state delocalisation requires some level of theoretical modelling. Early methods for the calculation of ZFS parameters of aromatic molecules were based on modelling of the π-electron distributions as a linear combination of atomic p-orbitals and calculating D as a sum of two-centre terms with weights given by the coefficients of the molecular orbitals occupied by the two unpaired electron spins [79]. These methods have since been further refined [35,80] and modified to include spin polarisation effects [81,82].

Density functional theory (DFT) and *ab initio* methods can also be used to predict the zero-field splitting and the calculation of the ZFS tensor is an option in most quantum chemical calculation packages. Studies on the spin-spin contribution to zero-field splitting in polyacenes revealed that while DFT underestimated the absolute D values, often by almost a factor of 2, the trend to smaller D with increased π-conjugation length was correctly reproduced [83,84]. A comparison of experimental D values with theoretical predictions using different levels of theory in ORCA [85] showed that the experimental results could best be reproduced by restricted open-shell calculations with the BP or B3LYP hybrid functionals and the EPRII [86] basis set [84]. The main reason for the relatively poor performance in the calculation of absolute D values by DFT is that the electron-correlation effects are not accurately described. Improved agreement between calculated and theoretical values for aromatic molecules can be obtained using multiconfigurational approaches that include the static π-electron correlation, but at a currently higher computational cost [83,84]. The comparison of experimental and calculated trends in ZFS is, however, often sufficient to estimate the extent of triplet state delocalisation.

More accurate determination of the extent of the triplet state wavefunction requires the measurement of the hyperfine couplings. The hyperfine coupling constants are determined by the spin density distribution of the system. Therefore, if complete delocalisation occurs over more than one unit in an oligomeric system, and the spin density distributions on each of the units can be considered identical, the hyperfine coupling constants of the oligomer, $A_{N,i}$, will be reduced compared to the monomeric unit, $A_{1,i}$, by a factor of one over the number of units N over which delocalisation occurs [87]:

$$A_{N,i} = \frac{1}{N} A_{1,i} \tag{9}$$

If the spin density is evenly distributed over all units and these units are all identical, this formula enables the quantification of delocalisation in a straightforward way. Even for uneven or asymmetrical spin density distributions, comparison of the hyperfine couplings with those of the monomeric unit can provide information on the characteristics of the distributions. For example, in the case of the special pair of *Rh. sphaeroides* the observation of two sets of reduced hyperfine couplings were interpreted in terms of a distribution with 60% of the spin density on one bacteriochlorophyll *a* and 40% on the other one [29].

The spin density distributions on individual units in oligomeric π-conjugated chains can differ from the spin density distribution of the isolated monomer due to the influence of the linkers or adjacent units. This leads to a partial breakdown of the main assumption behind the derivation of Eq. (9) and deviations from this predicted relationship may be observed. In that case, the interpretation of the experimental hyperfine couplings in terms of an overall triplet state spin density distribution can be aided by quantum chemical modelling [20,32,38]. The performance of DFT and *ab initio* methods in the prediction of hyperfine interactions is much better compared to the prediction of the zero-field splitting parameters and relatively accurate hyperfine coupling tensors can typically be obtained [38,88,89].

Information on delocalisation/exciton hopping can also be obtained from triplet kinetics, as demonstrated for example for porphyrin dimers in Ref. [17]. Modulation of either zero-field splitting parameters or ZFS tensor axes induced by exciton hopping

constitutes an effective spin-lattice relaxation mechanism. Therefore comparison of the relaxation properties of the monomeric unit and oligomers can indicate the presence of triplet-triplet energy transfer [17]. This mechanism does, however, not lead to changes in the spin-lattice relaxation time if hopping occurs between identical units with collinear ZFS tensors, such as in a linear oligomer or stacked coplanar supramolecular arrays.

4. Case study: triplet state delocalisation in linear porphyrin oligomers

Application of the methodologies described in the previous sections for the characterisation of triplet state delocalisation will be illustrated on the example of linear porphyrin chains designed to act as molecular wires [20,38]. The structures of the investigated butadiyne-linked aryl-substituted Zn porphyrin oligomers are shown in Fig. 1e. The EPR measurements were performed at 20 K in frozen MeTHF:pyridine solutions (0.1–0.2 mM) and the photoexcited triplet states were generated by excitation with a Nd:YAG laser (10 Hz, 5 ns pulses) at 532 nm.

4.1. TR-EPR: ZFS interaction and spin polarisation

The transient EPR spectra recorded for the linear porphyrin oligomers **Pn** with $n = 1$–6 are shown in Fig. 7. The different widths of the triplet state EPR spectra, corresponding to $2|D|$, indicate changes in the zero-field splitting interaction as a function of the oligomer length. The significantly different spin polarisations suggest changes in the selectivity of the population of different triplet state sublevels by ISC. The absolute values of the zero-field splitting D and E parameters as well as the relative sublevel populations were extracted by simulation of the EPR spectra using EasySpin [90] (see Fig. 7).

The D value increases significantly from **P1** to **P2**, followed by only slight further changes for the longer oligomers. The increase in D for **P2**, despite the increased π conjugation length, can be explained by a change in the sign of D from positive in the monomer to negative in the dimer, corresponding to a change from an oblate to a prolate spin density distribution (see Section 3.1). The change in the sign of D is associated with a shift of the axis of maximum dipolar coupling, assigned to Z by convention, from the out-of-plane axis in the monomer to the long-axis in the dimer. This was confirmed by magnetophotoselection experiments and is an indication for increased delocalisation in the porphyrin dimer [38].

Comparison of the principal values of the $\boldsymbol{D}$ tensor along the molecular axes shows that the zero-field splitting in the molecular plane (D_{aryl}, D_{triple}) is affected by the presence of a second porphyrin unit, while the out-of-plane contribution (D_{oop}) remains approximately constant. The fact that addition of further porphyrin units does hardly affect the zero-field splitting suggests a similar extent of triplet delocalisation from **P2** onwards.

Interpretation of the D values in terms of the point-dipole approximation, considering the change in the angular term of Eq. (4) due to the transition from an oblate to a prolate system, would yield average inter-electron distances of about 3.5 Å and 4.1 Å, for **P1** and the longer oligomers, respectively. Compared to the 6.9 Å *meso*-to-*meso* distance in a porphyrin, this could lead to the conclusion of localisation of the triplet state on a single porphyrin unit in all oligomers. However, calculation of the ZFS parameters by DFT (at the B3LYP/EPRII level) predicts similar relative changes in D and E as observed experimentally for triplet states delocalised over both porphyrin units in **P2** and delocalised mainly over the central porphyrin units in the longer oligomers [38].

The spin polarisation of the **P1** triplet state spectrum is in agreement with results on other zinc porphyrin systems. The preferential population of the out-of-plane (Z) sublevel has been attributed to a contribution of the zinc spin-orbit coupling to ISC [91,92]. The spin polarisation of the **P2** spectrum, on the other hand, indicates population of mainly the X sublevel. This can be explained by the same ISC mechanism, considering the shift of the ZFS Z axis from the out-of-plane axis in **P1** to the long axis of the molecule in **P2**, leading to the X axis being the new

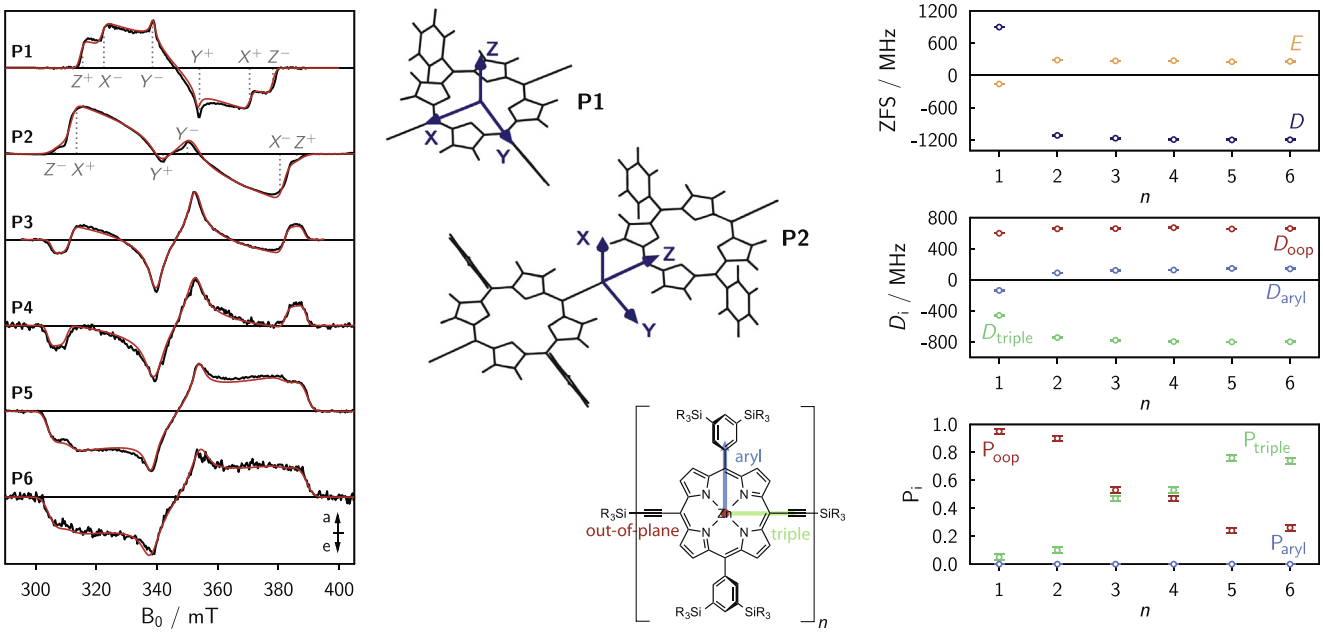

Fig. 7. *Left*: Experimental (black) and simulated (red) X-band transient EPR spectra of linear porphyrin chains (**P1**–**P6**) in MeTHF:pyridine 10:1 at 20 K; *Centre*: orientation of the ZFS tensor in the molecular frame for **P1** and **P2** as well as definition of the molecular axes *Right*: ZFS D and E parameters (*top*), eigenvalues of the ZFS tensor along the molecular axes (*middle*) and relative sublevel populations (*bottom*) as a function of the number (n) of porphyrin units. The ordering of the triplet sublevels was chosen as $|Z| > |X| > |Y|$, and the six canonical positions are indicated for **P1** and **P2**. For **P3**–**P6**, the same assignments as shown for **P2** are valid. The spectra recorded after laser excitation with unpolarised light at 532 nm were averaged up to 2 μs after the laser pulse [20]. (For interpretation of the references to colour in this figure legend, the reader is referred to the web version of this article.)

out-of-plane axis. The assignment could also be confirmed by magnetophotoselection and orientation-selective ENDOR (see below). The spin polarisation of the **P2** spectrum thus provides further confirmation of the sign change of *D*.

In the longer oligomers, the spin polarisation of the spectra indicates a progressive increase in the *Z* (long-axis) sublevel population. A comparison with the trends in spin polarisations observed for the corresponding free-base porphyrins has led to the proposal of an increased contribution of Herzberg-Teller vibronic coupling to ISC with increasing chain lengths and therefore increased vibrational freedom of the porphyrin oligomers [20].

4.2. Hyperfine spectroscopy: ^{1}H and ^{14}N hyperfine interactions

As discussed in Section 3.4, the measurement of the hyperfine couplings typically provides a more precise quantitative measure of the extent of triplet state delocalisation than the ZFS. The ^{1}H and ^{14}N hyperfine couplings in the porphyrin oligomers were therefore characterised by ENDOR and ESEEM/HYSCORE.

The ^{1}H Mims ENDOR spectra recorded for **P1** and **P2** at the six canonical field positions are shown in Fig. 8. Since the sign of the *D* value is known from magnetophotoselection experiments and DFT, the sign of the hyperfine couplings can be determined as explained in Section 3.3 based on the position of the ENDOR peaks with respect to the Larmor frequency in each transition-selective ENDOR spectrum. The distance between each ENDOR peak and the Larmor frequency corresponds to the hyperfine coupling along the selected ZFS axis. For **P1**, the largest hyperfine coupling is observed in the ENDOR spectra corresponding to the *Z* and *Y* orientations of the ZFS tensor and amounts to about −3 MHz. Comparison with the hyperfine tensors calculated by DFT allows assignment of this coupling to the β-proton adjacent to the triple bonds, H_1 (see Fig. 8), characterised by large couplings along the out-of-plane (*Z*) and aryl (*Y*) axes and a smaller coupling along the triple bond (*X*) axis. The smaller positive hyperfine couplings observed in the experimental ENDOR spectra could be assigned to the second type of β-protons, H_2, while the couplings of the protons on the aryl substituents are not sufficiently resolved to allow a clear assignment.

Inspection of the corresponding ENDOR spectra of **P2** reveals significant differences between the monomer and the dimer. All hyperfine interactions in **P2** are smaller compared to the respective couplings in **P1**: the largest couplings now amount to −1.5 MHz and are observed along the *X* and *Y* axes of the ZFS tensor. The reduction of the hyperfine couplings by a factor of two indicates delocalisation of the triplet state over both porphyrin units in the dimer. Additionally, for analogous field positions, e.g. the high-field *Y* position, the ENDOR peaks have shifted from one side of the Larmor frequency to the other. This is caused by the sign change of *D* that leads to a change in the assignment of the field positions to the $-1 \leftrightarrow 0$ or $0 \leftrightarrow +1$ triplet transitions, respectively. Finally, the observation of large hyperfine couplings along the *Z* and *Y* axes in **P1** and the *X* and *Y* axes in **P2** is explained by the reorientation of the ZFS tensor axes due to the sign change of *D*: in both cases they correspond to the out-of-plane and aryl substituent axes of the molecular frame. Again, a good agreement with the hyperfine couplings predicted by DFT was obtained [38]. In addition to quantifying triplet state delocalisation, the orientation-selective ENDOR measurements in conjunction with the DFT calculations have thus allowed determination of the orientation of the ZFS tensor with respect to the molecular frame for **P1** and **P2**, confirming the conclusions drawn based on the TR-EPR and magnetophotoselection data.

The extent of triplet state delocalisation in the longer oligomers was determined by comparison of the hyperfine coupling of H_1 along the axis of the aryl substituents, corresponding to the ZFS *Y* axis for both **P1** and the longer oligomers. The corresponding ENDOR spectra are compared in Fig. 9 (*left*) and show that the decrease of the hyperfine coupling by a factor of two from **P1** to **P2** is followed first by a small increase for **P3** and then by a progressive decrease for the longer oligomers. The experimental hyperfine couplings are compared to the couplings expected in case of complete delocalisation of the triplet state (grey line in Fig. 9, *right*). Assuming identical porphyrin units, a comparison of the measured hyperfine couplings of the oligomers with that of the monomer allows determination of the largest spin density contribution on a single porphyrin unit. In **P2**, the triplet state is completely delocalised, giving 50% of the monomer spin density on

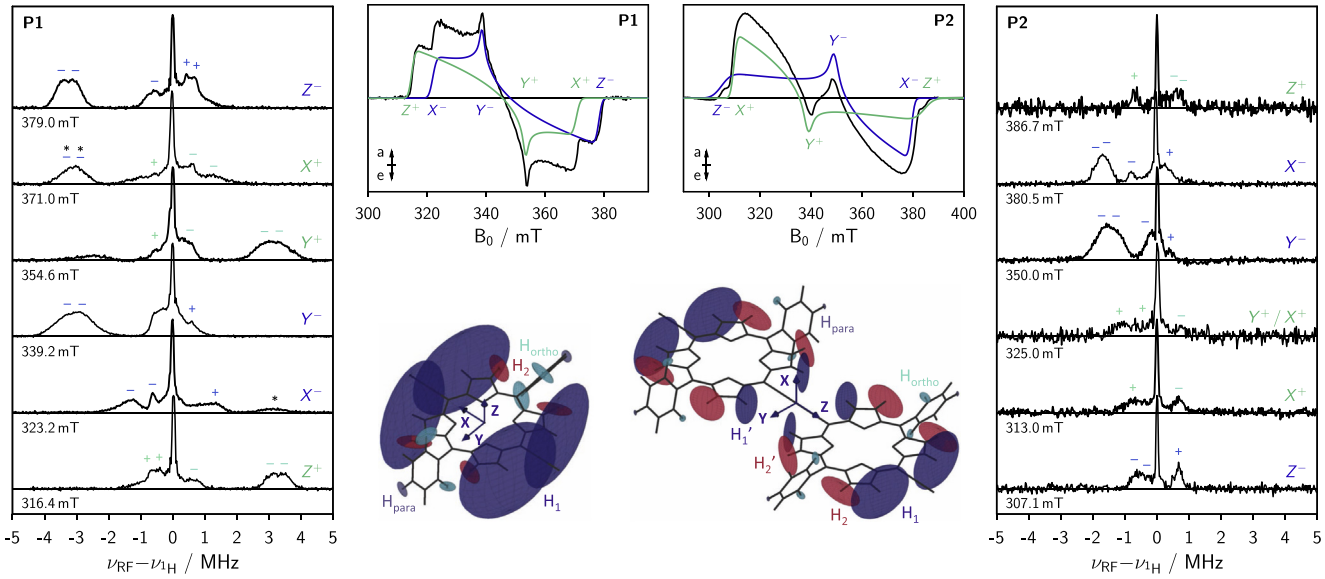

Fig. 8. Experimental ^{1}H Mims ENDOR spectra of **P1** (*left*) and **P2** (*right*) recorded at the canonical field positions at 20 K [38]. The signs of the hyperfine coupling constants of the $m_S = 0 \leftrightarrow m_S = +1$ (green) and the $m_S = -1 \leftrightarrow m_S = 0$ (blue) transitions are shown above the respective ENDOR peaks. The asterisks denote ENDOR peaks arising from residual contributions of other orientations (*e.g.* Z^- contribution to X^+). The triplet state EPR spectra with labelled canonical orientations and the simulations of the $m_S = 0 \leftrightarrow m_S = +1$ and $m_S = -1 \leftrightarrow m_S = 0$ subspectra are shown in the centre. The proton hyperfine tensors calculated at the B3LYP/EPRII level for **P1** and **P2** are also illustrated. (For interpretation of the references to colour in this figure legend, the reader is referred to the web version of this article.)

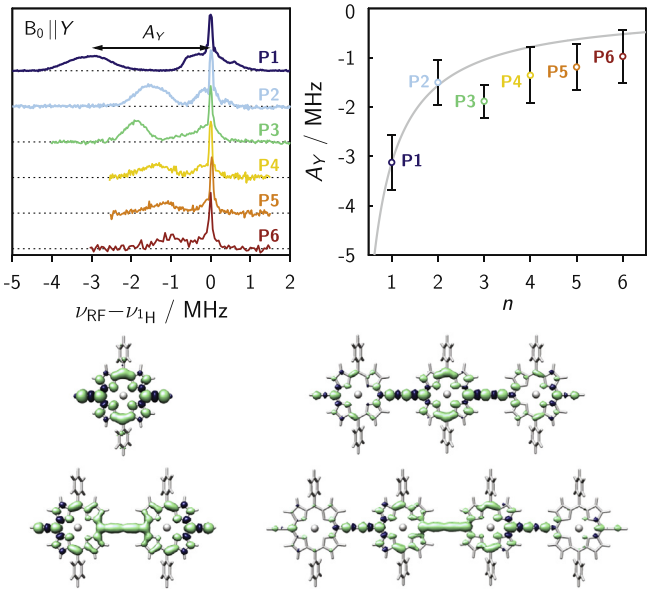

Fig. 9. Experimental ^{1}H Mims ENDOR spectra of **P1**–**P6** recorded at the Y^- field position at 20 K [20] (*left*) and hyperfine couplings of the H_1 protons along the *Y* axis of the ZFS tensor (A_Y) as a function of the oligomer size (*right*). The hyperfine couplings were determined by Gaussian fitting of the principal hyperfine peak in the experimental ENDOR spectra; the error bars indicate the full width at half-maximum (FWHM). The grey line corresponds to the theoretical n^{-1} relationship [87] for the hyperfine couplings expected in case of complete delocalisation. The B3LYP/EPRII spin density distributions for **P1**–**P4** are shown at the bottom.

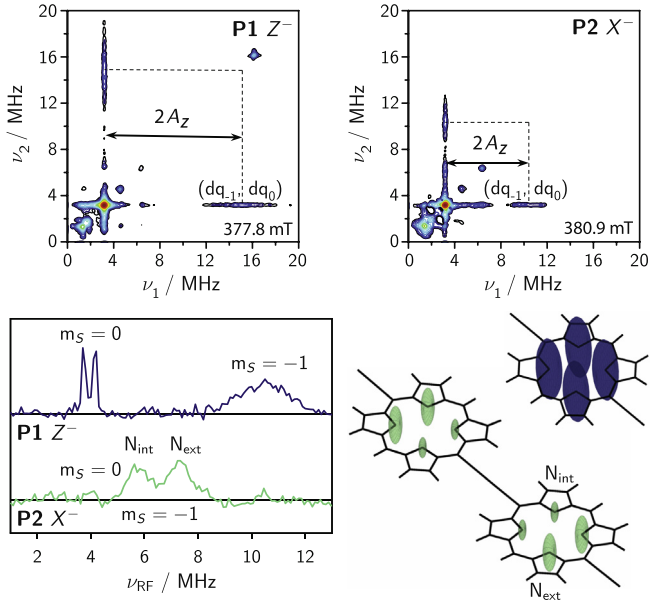

Fig. 10. X-band HYSCORE (*top*) and Q-band ENDOR (*bottom*) spectra recorded at 20 K at field positions corresponding to the out-of-plane orientation for **P1** (Z^-) and **P2** (X^-) [38]. The double-quantum peaks in the HYSCORE spectra are labelled. The **P1** ENDOR spectrum was recorded using the Davies ENDOR sequence and the **P2** ENDOR spectrum using Mims ENDOR summed over four different τ values (the presence of remaining blind spots leads to a reduced intensity of the transitions in the $m_S = 0$ manifold centred at about 4 MHz). A visualisation of the experimentally determined nitrogen hyperfine coupling tensors is shown for **P1** and **P2** on the bottom right.

each porphyrin unit, while the largest measured hyperfine couplings of **P3**–**P6** correspond to 60%, 45%, 40% and 34% of the monomer spin density, respectively. These results are in good agreement with DFT calculations predicting spin density distributions with larger contributions on the central porphyrin units as indicated for **P3** and **P4** in Fig. 9 (*bottom right*).

In addition to the proton hyperfine couplings, the nitrogen hyperfine couplings can provide the same information on triplet state delocalisation. The X-band HYSCORE and Q-band ENDOR data for **P1** and **P2** in Fig. 10 clearly show a shift of the largest nitrogen hyperfine coupling, corresponding to the out-of-plane orientation in porphyrin molecules, from the ZFS *Z* axis in **P1** to the *X* axis in **P2**. Additionally, a reduction of the magnitude of the coupling and splitting into two contributions is observed, indicating complete delocalisation with different hyperfine couplings for the external and internal nitrogen nuclei in **P2** [38]. HYSCORE and three-pulse ESEEM data for **P3** confirmed the conclusions drawn based on the ^{1}H ENDOR data. Analysis of the ^{14}N hyperfine interaction in the longer oligomers was prevented by the low triplet yield and the presence of the nuclear quadrupole interaction with a magnitude comparable to that of the hyperfine coupling.

4.3. Conclusions

In summary, the combination of TR-EPR and hyperfine techniques with quantum mechanical tools for the prediction of magnetic properties has allowed an in-depth characterisation of the photoexcited triplet states of this series of porphyrin oligomers. This study has shown that information on triplet state delocalisation is contained in the ZFS interaction and the spin polarisation of the EPR spectrum. However, an accurate interpretation of the experimental data in terms of the distribution of the triplet state wavefunction, and therefore the extent of delocalisation, required the measurement of the hyperfine couplings. The ZFS interaction contains the same information, but could only be interpreted by comparison of the experimental *D* and *E* values with results from DFT calculations.

5. Perspective/Outlook

Since triplet states are important intermediates in many photochemical reactions of biological and technological relevance, research involving the characterisation of their properties is expected to remain topical. In the last decades, the main driving force to study triplet state delocalisation were applications in solar energy harvesting, including processes like singlet fission or triplet-triplet photon up-conversion, and in molecular electronics. Systematic studies of the electronic structure of oligomeric and polymeric systems as a function of the molecular structure of the constituents and supramolecular geometry can provide insight into the factors governing triplet state delocalisation, leading to improved efficiencies of molecular electronics components and solar energy devices.

The understanding of triplet state properties, including their delocalisation, considerably improved with the development and the commercial availability of more sensitive (ENDOR) resonators [93–95] and the affordability of more stable laser systems with variable repetition rate. In addition, the availability of wavelength tunable laser excitation sources (OPOs) opens up the possibility to selectively probe specific molecular conformations [42] as well as to selectively excite specific chromophores of a molecular assembly or specific (excited state) reaction intermediates [96]. In case of a reasonable triplet yield, high quality data can nowadays be acquired in a relatively straightforward manner.

While in earlier days, triplet state EPR studies were mainly focussed on the characterisation of the triplet states themselves, instrumental and methodological developments now allow the triplet state to be used as a probe to gain further knowledge about more complex molecular systems or mechanisms. For example,

EPR investigations on triplet states in light-harvesting complexes and photosynthetic reaction centres have provided insight into energy transfer mechanisms at the basis of light harvesting and photoprotection [23,24,26,28–30,32,67,97–103]. Recently, photoexcited triplet states have also been proposed as spin labels for distance measurements in biomacromolecules [104–107]. For such experiments, an accurate knowledge of the spin density distribution is necessary to precisely determine the distance distribution and therefore obtain reliable information on the structure and dynamics of the investigated systems.

Most of the experimental results on triplet state delocalisation obtained thus far seem to suggest that triplet states are more spatially confined than the corresponding singlet states [19,108–110]. Although often noted, this phenomenon is still poorly understood. Given the methodological improvements in the last decades mentioned above, which enable a thorough and quantitative characterisation of triplet state properties by EPR, we may now be in the position to answer some of the questions regarding the factors influencing the extent of triplet state delocalisation. Molecules with different geometries and shapes are currently being investigated in systematic studies with the aim to explore the influence of different factors such as geometry, conformation and electronic symmetry on the average delocalisation length of the excited triplet state.

Information on triplet state delocalisation is contained both in the ZFS and hyperfine interactions and approaches to extract the extent of delocalisation from either are well established. Yet, the case study in Section 4 illustrated that it may not be possible in all cases to directly determine the extent of delocalisation only based on the magnitude of the ZFS parameter *D*. The analysis of the zero-field splitting parameters and results from hyperfine experiments should in principle yield identical information, however, for an accurate interpretation of the ZFS parameters, the orientation of the ZFS tensor within the molecular frame needs to be known. To determine this tensor orientation, additional measurements or calculations are required.

Theoretical input from quantum chemical calculations is not only useful to determine the tensor orientations, but may also be required for interpretation of the experimental ZFS splitting parameters as well as a complete assignment and interpretation of the electron-nuclear couplings observed in hyperfine experiments. DFT calculations are particularly suited for this purpose since, owing to recent improvements [111,112], the challenging computation of EPR parameters has become comparatively cheap and accurate. While hyperfine couplings can usually be predicted with fairly good accuracy, the absolute values obtained for ZFS parameters from DFT can deviate quite significantly from the experimental ones. However, parameter trends seem to be generally reliable. Improved agreement between experimental and calculated ZFS values can be obtained using multiconfigurational methods and current efforts aimed at improving the implementation and increasing the efficiency of these methods [113–115] will likely make them more widely applicable in the future.

The main experimental challenge in the study of triplet state delocalisation is the drastic decrease in triplet yield often observed with increasing oligomer length [20]. Low triplet yields automatically imply very weak signal intensities and might in some cases even prevent the feasibility of a particular triplet state experiment. Unfortunately, the triplet yield cannot easily be influenced without changing the chemistry or excited state mechanism, as is done, for instance, by core substitution with heavy atoms or addition of triplet sensitisers. A possibility to influence the triplet yield in compounds such as porphyrins might be to introduce a heavier central metal in a diamagnetic coordination state, such as Pd(II) or Pt(II). Intersystem crossing should be favoured in this case, however, the insertion of heavy metals might complicate the data analysis since the consideration of spin-orbit coupling and relativistic effects becomes increasingly relevant. In particular, the interpretation of the ZFS parameters presented in this article relies on the negligibility of any additional contributions to the ZFS apart from the spin-spin interaction.

Considering the triplet yield of the samples as immutable, future developments might allow a further enhancement of the measurement sensitivity by either increasing the sensitivity of the resonator/detection or the efficiency of the microwave excitation of the sample. The introduction of arbitrarily shaped pulses to EPR, for example, has already been shown to lead to significant improvements in pulse EPR sensitivity and to provide the opportunity for development of more efficient or more informative experiments [116–118].

Acknowledgements

We thank the EPSRC (EPL011972/1) and the ERC (grant 320969) for support. The authors would like to acknowledge the use of the University of Oxford Advanced Research Computing (ARC) facility in carrying out this work.

References

[1] B.J. Walker, A.J. Musser, D. Beljonne, R.H. Friend, Singlet exciton fission in solution, Nat. Chem. 5 (2013) 1019–1024.
[2] A. Rao, P.C.Y. Chow, S. Gélinas, C.W. Schlenker, C.-Z. Li, H.-L. Yip, A.K.-Y. Jen, D. S. Ginger, R.H. Friend, The role of spin in the kinetic control of recombination in organic photovoltaics, Nature 500 (2013) 435–440.
[3] J.M. Tour, Molecular electronics. Synthesis and testing of components, Acc. Chem. Res. 33 (2000) 791–804.
[4] S.A. Wolf, D.D. Awschalom, R.A. Buhrman, J.M. Daughton, S. von Molnár, M.L. Roukes, A.Y. Chtchelkanova, D.M. Treger, Spintronics: a spin-based electronics vision for the future, Science 294 (2001) 1488–1495.
[5] J.S. Wilson, A.S. Dhoot, A.J.A.B. Seeley, M.S. Khan, A. Köhler, R.H. Friend, Spin-dependent exciton formation in π-conjugated compounds, Nature 413 (2001) 828–831.
[6] M. Wohlgenannt, X.M. Jiang, Z.V. Vardeny, R.A.J. Janssen, Conjugation-length dependence of spin-dependent exciton formation rates in π-conjugated oligomers and polymers, Phys. Rev. Lett. 88 (2002) 197401/1-4.
[7] S. Karabunarliev, E.R. Bittner, Spin-dependent electron-hole capture kinetics in luminescent conjugated polymers, Phys. Rev. Lett. 90 (2003) 057402/1–057402/4.
[8] N.C. Erickson, R.J. Holmes, Investigating the role of emissive layer architecture on the exciton recombination zone in organic light-emitting devices, Adv. Funct. Mater. 23 (2013) 5190–5198.
[9] J.-H. Ha, H.S. Cho, J.K. Song, D. Kim, N. Aratani, A. Osuka, Excitonic coupling strength and coherence length in the singlet and triplet excited states of meso-meso directly linked Zn(II) porphyrin arrays, ChemPhysChem 5 (2004) 57–67.
[10] A. Köhler, H. Bässler, What controls triplet exciton transfer in organic semiconductors?, J Mater. Chem. 21 (2011) 4003–4011.
[11] M. Tabachnyk, B. Ehrler, S. Gélinas, M.L. Böhm, B.J. Walker, K.P. Musselman, N. C. Greenham, R.H. Friend, A. Rao, Resonant energy transfer of triplet excitons from pentacene to PbSe nanocrystals, Nat. Mater. 13 (2014) 1033–1038.
[12] G.H. Gelinck, J.J. Piet, J.M. Warman, The polarizability of triplet excitons on oligothiophene chains, Synth. Met. 101 (1999) 553–554.
[13] S.L. Bayliss, K.J. Thorley, J.E. Anthony, H. Bouchiat, N.C. Greenham, A.D. Chepelianskii, Localization length scales of triplet excitons in singlet fission materials, Phys. Rev. B 92 (2015) 115432/1-7.
[14] R.H. Clarke, D.R. Hobart, W.R. Leenstra, The triplet state of the chlorophyll dimer, J. Am. Chem. Soc. 101 (1979) 2416–2423.
[15] R.H. Clarke, Triplet State Optically Detected Magnetic Resonance Spectroscopy: Techniques and Applications to Biophysical Systems, John Wiley & Sons, Inc, 1982.
[16] D. Carbonera, Optically detected magnetic resonance (ODMR) of photoexcited triplet states, Photosynth. Res. 102 (2009) 403–414.
[17] P. Jaegermann, M. Plato, B. von Maltzan, K. Möbius, Time-resolved EPR study of exciton hopping in porphyrin dimers in their photoexcited triplet state, Mol. Phys. 78 (1993) 1057–1074.
[18] M. Bennati, A. Grupp, M. Mehring, Pulsed EPR on the photoexcited triplet state of C_{60} fullerene, Chem. Phys. Lett. 200 (1992) 440–444.
[19] P.J. Angiolillo, V.S.-Y. Lin, J.M. Vanderkooi, M.J. Therien, EPR spectroscopy and photophysics of the lowest photoactivated triplet state of a series of highly conjugated (porphinato) Zn arrays, J. Am. Chem. Soc. 117 (1995) 12514–12527.
[20] C.E. Tait, P. Neuhaus, M.D. Peeks, H.L. Anderson, C.R. Timmel, Transient EPR reveals triplet state delocalization in a series of cyclic and linear π-conjugated porphyrin oligomers, J. Am. Chem. Soc. 137 (2015) 8284–8293.

[21] H. Levanon, J.R. Norris, The photoexcited triplet state and photosynthesis, Chem. Rev. 78 (1978) 185–198.
[22] M.C. Thurnauer, ESR study of the photoexcited triplet state in photosynthetic bacteria, Rev. Chem. Intermed. 100 (1979) 197–231.
[23] W. Lubitz, F. Lendzian, R. Bittl, Radicals, radical pairs and triplet states in photosynthesis, Acc. Chem. Res. 35 (2002) 313–320.
[24] A. De Groot, R. Evelo, A.J. Hoff, R. De Beer, H. Scheer, Electron spin echo envelope modulation (ESEEM) spectroscopy of the triplet state of the primary donor of ^{14}N and ^{15}N bacterial photosynthetic reaction centers and of ^{14}N and ^{15}N bacteriochlorophyll *a*, Chem. Phys. Lett. 118 (1985) 48–54.
[25] J.R. Norris, D.E. Budil, P. Gast, C.-H. Chang, O. El-Kabbani, M. Schiffer, Correlation of paramagnetic states and molecular structure in bacterial photosynthetic reaction centers: The symmetry of the primary electron donor in *Rhodopseudomonas viridis* and *Rhodobacter sphaeroides* R-26, Proc. Natl. Acad. Sci. U.S.A. 86 (1989) 4335–4339.
[26] D.E. Budil, M.C. Thurnauer, The chlorophyll triplet state as a probe of structure and function in photosynthesis, Biochem. Biophys. Acta 1057 (1991) 1–41.
[27] M. Di Valentin, C.W.M. Kay, G. Giacometti, K. Möbius, A time-resolved electron nuclear double resonance study of the photoexcited triplet state of P680 in isolated reaction centers of photosystem II, Chem. Phys. Lett. 248 (1996) 434–441.
[28] M. Huber, A.A. Doubinskii, C.W.M. Kay, K. Möbius, ENDOR on the triplet state of the primary electron donor in the photosynthetic bacterium *Rhodobacter sphaeroides* – one step forward in a still unfinished story, Appl. Magn. Reson. 13 (1997) 473–485.
[29] F. Lendzian, R. Bittl, W. Lubitz, Pulsed ENDOR of the photoexcited triplet states of bacteriochlorophyll *a* and of the primary donor P865 in reaction centers of *Rhodobacter sphaeroides* R-26, Photosynth. Res. 55 (1998) 189–197.
[30] R. Bittl, E. Schlodder, I. Geisenheimer, W. Lubitz, R.J. Cogdell, Transient EPR and absorption studies of carotenoid triplet formation in purple bacterial antenna complexes, J. Phys. Chem. B 105 (2001) 5525–5535.
[31] F. Lendzian, R. Bittl, A. Telfer, W. Lubitz, Hyperfine structure of the photoexcited triplet state ^{3}P680 in plant PS II reaction centres as determined by pulse ENDOR spectroscopy, Biochim. Biophys. Acta 1605 (2003) 35–46.
[32] A. Marchanka, W. Lubitz, M. Plato, M. van Gastel, Comparative ENDOR study at 34 GHz of the triplet state of the primary donor in bacterial reaction centers of *Rb. sphaeroides* and *Bl. viridis*, Photosynth. Res. 120 (2014) 99–111.
[33] I. Sieckmann, K. Brettel, C. Bock, A. van der Est, D. Stehlik, Transient electron paramagnetic resonance of the triplet state of P_{700} in photosystem I: evidence for triplet delocalization at room temperature, Biochemistry 32 (1993) 4842–4847.
[34] V. Hamacher, J. Wrachtrap, B. von Maltzan, M. Plato, K. Möbius, EPR and ENDOR study of porphyrins and their covalently linked dimers in the photoexcited triplet state, Appl. Magn. Reson. 4 (1993) 297–319.
[35] M. Bennati, N. Németh, P.R. Surján, M. Mehring, Zero-field-splitting and π-electron spin densities in the lowest excited triplet state of oligothiophenes, J. Chem. Phys. 105 (1996) 4441–4447.
[36] P.J. Angiolillo, K. Susumu, H.T. Uyeda, V.S.-Y. Lin, R. Shediac, M.J. Therien, Trends in triplet excitation delocalization in highly conjugated (porphinato) zinc(II) arrays probed by EPR spectroscopy, Synth. Met. 116 (2001) 247–253.
[37] P.J. Angiolillo, H.T. Uyeda, T.V. Duncan, M.J. Therien, Impact of electronic asymmetry on photoexcited triplet-state spin distributions in conjugated porphyrin oligomers probed via EPR spectroscopy, J. Phys. Chem. B 108 (2004) 11893–11903.
[38] C.E. Tait, P. Neuhaus, H.L. Anderson, C.R. Timmel, Triplet state delocalization in a conjugated porphyrin dimer probed by transient electron paramagnetic resonance techniques, J. Am. Chem. Soc. 137 (2015) 6670–6679.
[39] R. Shediac, M.H.B. Gray, H.T. Uyeda, R.C. Johnson, J.T. Hupp, P.J. Angiolillo, M.J. Therien, Singlet and triplet excited states of emissive, conjugated bis (porphyrin) compounds probed by optical and EPR spectroscopic methods, J. Am. Chem. Soc. 122 (2000) 7017–7033.
[40] P.J. Angiolillo, J. Rawson, P.R. Frail, M.J. Therien, The evolution of spin distribution in the photoexcited triplet state of ethyne-elaborated porphyrins, Chem. Commun. 49 (2013) 9722–9724.
[41] A. Berman, H. Levanon, E. Vogel, N. Jux, Triplet spin alignment of stretched porphycenes, Chem. Phys. Lett. 211 (1993) 549–554.
[42] C.E. Tait, P. Neuhaus, M.D. Peeks, H.L. Anderson, C.R. Timmel, Excitation wavelength-dependent EPR study on the influence of the conformation of multiporphyrin arrays on triplet state delocalization, Phys. Chem. Chem. Phys. 18 (2016) 5275–5280.
[43] S. Richert, M. Peeks, C.E. Tait, H.L. Anderson, C.R. Timmel, Photogenerated triplet states in supramolecular porphyrin ladder assemblies: an EPR study, Phys. Chem. Chem. Phys. 18 (2016) 24171–24175.
[44] S. Richert, G. Bullard, J. Rawson, P.J. Angiolillo, M.J. Therien, C.R. Timmel, On the importance of electronic symmetry for triplet state delocalization, J. Am. Chem. Soc. (2017), http://dx.doi.org/10.1021/jacs.7b01204.
[45] H. Levanon, Spin polarized triplets oriented in liquid crystals, Rev. Chem. Intermed. 8 (1987) 287–320.
[46] O. Gonen, H. Levanon, Line-shape analysis of transient triplet electron paramagnetic resonance spectra. Application to porphyrins and chlorophylls in nematic uniaxial liquid crystals, J. Phys. Chem. 88 (1984) 4223–4228.
[47] O. Gonen, H. Levanon, Energy transfer and fine structure axes determination in a hybrid porphyrin dimer oriented in a liquid crystal: time resolved triplet EPR spectroscopy, J. Chem. Phys. 84 (1986) 4132–4141.
[48] M.D.E. Forbes, L.E. Jarocha, S.-Y. Sim, V.F. Tarasov, Time-resolved electron paramagnetic resonance spectroscopy: history, technique, and application to supramolecular and macromolecular chemistry, in: Advances in Physical Organic Chemistry, Advances in Physical Organic Chemistry, 47, Elsevier, 2013, pp. 1–83 (Chapter 1).
[49] R. Zeng, J. Van Tol, A. Deal, H.A. Frank, D.E. Budil, Primary donor triplet state *g*-tensor in photosynthetic reaction centers of *Rhodobacter sphaeroides* R-26 observed by transient 240 GHz electron paramagnetic resonance, J. Phys. Chem. B 107 (2003) 4624–4631.
[50] H. Levanon, K. Möbius, Advanced EPR spectroscopy on electron transfer processes in photosynthesis and biomimetic model systems, Annu. Rev. Biophys. Biomol. Struct. 26 (1997) 495–540.
[51] C.W.M. Kay, G. Elger, K. Möbius, The photoexcited triplet state of free-base porphycene: a time-resolved EPR and electron spin echo investigation, Phys. Chem. Chem. Phys. 1 (1999) 3999–4002.
[52] T.S. Lin, Electron spin echo spectroscopy of organic triplets, Chem. Rev. 84 (1984) 1–15.
[53] H. Seidel, M. Mehring, D. Stehlik, Room-temperature kinetics of the photoexcited triplet state of acridine in fluorene crystals as obtained from electron spin echo studies, Chem. Phys. Lett. 104 (1984) 552–559.
[54] C.E. Tait, P. Neuhaus, H.L. Anderson, C.R. Timmel, D. Carbonera, M. Di Valentin, HYSCORE on photoexcited triplet states, Appl. Magn. Reson. 46 (2015) 389–409.
[55] H. Seidel, M. Mehring, D. Stehlik, Electron spin echo envelope modulation (ESEEM) caused by ^{14}N and ^{2}D hyperfine interactions in the triplet state of acridine at room temperature, J. Chem. Phys. 83 (1985) 956–961.
[56] W.J. Buma, E.J.J. Groenen, J. Schmidt, R. de Beer, An electron spin-echo envelope modulation study of the lowest triplet state of pyridine-d_5: spin-density distribution and structure, J. Chem. Phys. 91 (1989) 6549–6566.
[57] K. Maeda, personal communication.
[58] T. Maly, T. Prisner, Relaxation filtered hyperfine spectroscopy (REFINE), J. Magn. Reson. 170 (2004) 88–96.
[59] C.P.J. Poole, H.A. Farach, W.K. Jackson, Standardization of convention for zero field splitting parameters, J. Chem. Phys. 61 (1974) 2220–2221.
[60] M.A. El-Sayed, Multiple resonance techniques in the study of the magnetic, radiative and non-radiative properties of the triplet state, Pure Appl. Chem. 24 (1970) 475–493.
[61] A.W. Hornig, J.S. Hyde, Paramagnetic resonance in triplet naphthalene at liquid helium temperatures, Mol. Phys 6 (1963) 33–41.
[62] H. Schuch, F. Seiff, R. Furrer, K. Möbius, K.P. Dinse, Direct determination of the absolute sign of the triplet zero-field parameter *D* by high resolution optical detection of ESR, Z. Naturforsch. 29a (1974) 1543–1547.
[63] M.C. Thurnauer, J.R. Norris, Magnetophotoselection applied to the triplet state observed by EPR in photosynthetic bacteria, Biochem. Biophys. Res. Commun. 73 (1976) 501–506.
[64] M.C. Thurnauer, J.R. Norris, The ordering of the zero field triplet spin sublevels in the chlorophylls. A magnetophotoselection study, Chem. Phys. Lett. 47 (1977) 100–105.
[65] J.A. Weil, J.R. Bolton, Electron Paramagnetic Resonance, second edition., John Wiley & Sons, Inc., 2007.
[66] R.C. Stevenson, Triplet state EPR spectra, J. Magn. Reson. 57 (1984) 24–42.
[67] M.C. Thurnauer, J.J. Katz, J.R. Norris, The triplet state in bacterial photosynthesis: possible mechanisms of the primary photo-act, Proc. Natl. Acad. Sci. USA 72 (1975) 3270–3274.
[68] M.A. El-Sayed, D.S. Tinti, E.M. Yee, Conservation of spin direction and production of spin alignment in triplet-triplet energy transfer, J. Chem. Phys. 51 (1969) 5721–5723.
[69] K. Akiyama, S. Tero-Kubota, T. Ikoma, Y. Ikegami, Spin polarization conservation during intramolecular triplet-triplet energy transfer studied by time-resolved EPR spectroscopy, J. Am. Chem. Soc. 116 (1994) 5324–5327.
[70] M. Di Valentin, C.E. Tait, E. Salvadori, S. Ceola, H. Scheer, R.G. Hiller, D. Carbonera, Conservation of spin polarization during triplet-triplet energy transfer in reconstituted peridinin-chlorophyll-protein complexes, J. Phys. Chem. B 115 (2011) 13371–13380.
[71] M. Asano-Someda, T. Ichino, Y. Kaizu, Triplet-triplet intramolecular energy transfer in a covalently linked copper (II) porphyrin-free base porphyrin hybrid dimer: a time-resolved ESR study, J. Phys. Chem. A 101 (1997) 4484–4490.
[72] D. Carbonera, M. Di Valentin, G. Agostini, G. Giacometti, P.A. Liddell, D. Gust, A.L. Moore, T.A. Moore, Energy transfer and spin polarization of the carotenoid triplet state in synthetic carotenoporphyrin dyads and in natural antenna complexes, Appl. Magn. Reson. 13 (1997) 487–504.
[73] F. Lendzian, H. Van Willigen, S. Sastry, K. Möbius, H. Scheer, R. Feick, Proton ENDOR study of the photoexcited triplet state P^T in *Rps. Sphaeroides* R-26 photosynthetic reaction centres, Chem. Phys. Lett. 118 (1985) 145–150.
[74] A.A. Doubinskii, Y.S. Lebedev, K. Möbius, ENDOR amplitudes of triplet state molecules: I. Electric-circuit analogy treatment, Appl. Magn. Reson. 13 (1997) 439–457.
[75] A.A. Doubinskii, Y.S. Lebedev, K.M. Salikhov, K. Möbius, ENDOR amplitudes of triplet state molecules: II. Orientational dependence of the ν_p frequency line and S-T_0 mixing, Appl. Magn. Reson. 13 (1997) 459–471.
[76] C. Riplinger, J.P.Y. Kao, G.M. Rosen, V. Kathirvelu, G.R. Eaton, S.S. Eaton, A. Kutateladze, F. Neese, Interaction of radical pairs through-bond and through-space: scope and limitations of the point-dipole approximation in electron paramagnetic resonance spectroscopy, J. Am. Chem. Soc. 131 (2009) 10092–10106.

[77] H. Hayashi, S. Iwata, S. Nagakura, ESR spectra of the charge-transfer triplet states of some molecular complexes, J. Chem. Phys. 50 (1969) 993–1000.
[78] T.K. Chandrashekar, H. van Willigen, ESR study of photoexcited triplets of some tetra(4-sulfonatophenyl) porphyrin dimers, Chem. Phys. Lett. 106 (1984) 237–241.
[79] M. Gouterman, W. Moffitt, Origin of zero-field splittings in triplet states of aromatic hydrocarbons, J. Chem. Phys. 30 (1959) 1369–1371.
[80] J. Visser, E.J.J. Groenen, The fine-structure in the lowest triplet state of C_{60} and C_{70}, Chem. Phys. Lett. 356 (2002) 43–48.
[81] M. van Gastel, The effect of spin polarization on zero field splitting parameters in paramagnetic π-electron molecules, J. Chem. Phys. 131 (2009) 124111/1–124111/7.
[82] M. van Gastel, Zero-field splitting of the lowest excited triplet states of C_{60} and C_{70} and benzene, J. Phys. Chem. A 114 (2010) 10864–10870.
[83] O. Loboda, B. Minaev, O. Vahtras, B. Schimmelpfennig, H. Ågren, K. Ruud, D. Jonsson, Ab initio calculations of zero-field splitting parameters in linear polyacenes, Chem. Phys. 286 (2003) 127–137.
[84] S. Sinnecker, F. Neese, Spin-spin contributions to the zero-field splitting tensor in organic triplets, carbenes and biradicals – a density functional and ab initio study, J. Phys. Chem. A 110 (2006) 12267–12275.
[85] F. Neese, The ORCA program system, Wiley Interdiscip. Rev.: Comput. Mol. Sci. 2 (2012) 73–78.
[86] V. Barone, Structure, magnetic properties and reactivities of open-shell species from density functional and self-consistent hybrid methods, in: D.P. Chong (Ed.), Recent Advances in Density Functional Methods, Part I, World Scientific, Singapore, 1996, pp. 287–334 (Chapter 8).
[87] J.R. Norris, R.A. Uphaus, H.L. Crespi, J.J. Katz, Electron spin resonance of chlorophyll and the origin of signal I in photosynthesis, Proc. Natl. Acad. Sci. U.S.A. 68 (1971) 625–628.
[88] J. Niklas, T. Schulte, S. Prakash, M. Van Gastel, E. Hofmann, W. Lubitz, Spin-density distribution of the carotenoid triplet state in the peridinin-chlorophyll-protein antenna. A Q-band pulse electron-nuclear double resonance and density functional theory study, J. Am. Chem. Soc. 129 (2007) 15442–15443.
[89] A. Marchanka, W. Lubitz, M. van Gastel, Spin density distribution of the excited triplet state of bacteriochlorophylls. Pulsed ENDOR and DFT studies, J. Phys. Chem. B 113 (2009) 6917–6927.
[90] S. Stoll, A. Schweiger, EasySpin, a comprehensive software package for spectral simulation and analysis in EPR, J. Magn. Reson. 178 (2006) 42–55.
[91] R.L. Ake, M. Gouterman, Porphyrins XIV. Theory for the luminescent state in VO, Co, Cu complexes, Theoret. Chim. Acta 15 (1969) 20–42.
[92] W.G. van Dorp, W.H. Schoemaker, M. Soma, J.H. Van der Waals, The lowest triplet state of free base porphin, Mol. Phys. 30 (1975) 1701–1721.
[93] Y. Grishin, C.W.M. Kay, A.A. Doubinskii, K. Möbius, A novel loop-gap resonator probehead for EPR and ENDOR at X-band, Appl. Magn. Reson. 13 (1997) 387–392.
[94] C.W.M. Kay, Y.A. Grishin, S. Weber, K. Möbius, An improved TM_{110} resonator for continuous-wave ENDOR studies at X-band, Appl. Magn. Reson. 31 (2007) 599–609.
[95] K. Möbius, A. Savitsky, W. Lubitz, M. Plato, Möbius-Hückel topology switching in expanded porphyrins: EPR, ENDOR, and DFT studies of doublet and triplet open-shell systems, Appl. Magn. Reson. 47 (2016) 757–780.
[96] L. Kobr, D.M. Gardner, A.L. Smeigh, S.M. Dyar, S.D. Karlen, R. Carmieli, M.R. Wasielewski, Fast photodriven electron spin coherence transfer: a quantum gate based on a spin exchange J-jump, J. Am. Chem. Soc. 134 (2012) 12430–12433.
[97] W.J. Buma, R.G. Evelo, E.J.J. Groenen, A.J. Hoff, H.M. Nan, J. Schmidt, The reaction center triplet state of the photosynthetic bacterium *Rhodobacter sphaeroides* R26: electron spin echo spectroscopy of a single crystal, Chem. Phys. Lett. 142 (1987) 231–236.
[98] M. Kammel, J. Kern, W. Lubitz, R. Bittl, Photosystem II single crystals studied by transient EPR: The light-induced triplet state, Biochim. Biophys. Acta 1605 (2003) 47–54.
[99] A. Marchanka, M. Paddock, W. Lubitz, M. van Gastel, Low-temperature pulsed EPR study at 34 GHz of the triplet states of the primary electron donor P865 and the carotenoid in native and mutant bacterial reaction centers of *Rhodobacter sphaeroides*, Biochemistry 46 (2007) 14782–14794.
[100] M. Di Valentin, S. Ceola, G. Agostini, G.M. Giacometti, A. Angerhofer, O. Crescenzi, V. Barone, D. Carbonera, Pulse ENDOR and density functional theory on the peridinin triplet state involved in the photo-protective mechanism in the peridinin-chlorophyll *a*-protein from *Amphidinium carterae*, Biochim. Biophys. Acta 1777 (2008) 295–307.
[101] M. Di Valentin, E. Salvadori, S. Ceola, D. Carbonera, Pulsed EPR and ENDOR on the peridinin triplet state involved in the photoprotective mechanism in peridinin-chlorophyll *a*-proteins, Appl. Magn. Reson. 37 (2009) 191–205.
[102] M. Di Valentin, E. Salvadori, V. Barone, D. Carbonera, Unravelling electronic and structural requisites of triplet-triplet energy transfer by advanced electron paramagnetic resonance and density functional theory, Mol. Phys. 111 (2013) 2914–2932.
[103] M. Di Valentin, C.E. Tait, E. Salvadori, L. Orian, A. Polimeno, D. Carbonera, Evidence for water-mediated triplet-triplet energy transfer in the photoprotective site of the peridinin-chlorophyll *a*-protein, Biochim. Biophys. Acta 1837 (2014) 85–97.
[104] M. Di Valentin, M. Albertini, E. Zurlo, M. Gobbo, D. Carbonera, Porphyrin triplet state as a potential spin label for nanometer distance measurements by PELDOR spectroscopy, J. Am. Chem. Soc. 136 (2014) 6582–6585.
[105] M. Di Valentin, M.G. Dal Farra, L. Galazzo, M. Albertini, T. Schulte, E. Hofmann, D. Carbonera, Distance measurements in peridinin-chlorophyll *a*-protein by light-induced PELDOR spectroscopy. Analysis of triplet state localization, Biochim. Biophys. Acta 1857 (2016) 1909–1916.
[106] C. Hintze, D. Bücker, S. Domingo Köhler, G. Jeschke, M. Drescher, Laser-induced magnetic dipole spectroscopy, J. Phys. Chem. Lett. 7 (2016) 2204–2209.
[107] M. Di Valentin, M. Albertini, M.G. Dal Farra, E. Zurlo, L. Orian, A. Polimeno, M. Gobbo, D. Carbonera, Light-induced porphyrin-based spectroscopic ruler for nanometer distance measurements, Chem. Eur. J. 22 (2016) 17204–17214.
[108] D. Beljonne, H.F. Wittmann, A. Köhler, S. Graham, M. Younus, J. Lewis, P.R. Raithby, M.S. Khan, R.H. Friend, J.L. Brédas, Spatial extent of the singlet and triplet excitons in transition metal-containing poly-ynes, J. Chem. Phys. 105 (1996) 3868–3877.
[109] J.J. Piet, P.N. Taylor, H.L. Anderson, A. Osuka, J.M. Warman, Excitonic interactions in the singlet and triplet excited states of covalently linked zinc porphyrin dimers, J. Am. Chem. Soc. 122 (2000) 1749–1757.
[110] J.J. Piet, P.N. Taylor, B.R. Wegewijs, H.L. Anderson, A. Osuka, J.M. Warman, Photoexcitations of covalently bridged zinc porphyrin oligomers: Frenkel versus Wannier-Mott type excitons, J. Phys. Chem. B 105 (2001) 97–104.
[111] F. Neese, The ORCA program system, Wiley Interdiscip. Rev.: Comput. Mol. Sci. 2 (2012) 73–78.
[112] F. Neese, Calculation of the zero-field splitting tensor on the basis of hybrid density functional and Hartree-Fock theory, J. Chem. Phys. 127 (2007) 164112/1–164112/9.
[113] A. Kumar Dutta, F. Neese, R. Izsák, Towards a pair natural orbital coupled cluster method for excited states, J. Chem. Phys. 145 (2016) 034102/1–034102/8.
[114] D. Datta, S. Kossmann, F. Neese, Analytic energy derivatives for the calculation of the first-order molecular properties using the domain-based local pair-natural orbital coupled-cluster theory, J. Chem. Phys. 145 (2016), 114101/1-18.
[115] L. Veis, A. Antalík, J. Brabec, F. Neese, O. Legeza, J. Pittner, Coupled cluster method with single and double excitations tailored by matrix product state wave functions, J. Phys. Chem. Lett. 7 (2016) 4072–4078.
[116] G. Jeschke, S. Pribitzer, A. Doll, Coherence transfer by passage pulses in electron paramagnetic resonance spectroscopy, J. Phys. Chem. B 119 (2015) 13570–13582.
[117] G. Jeschke, Wideband frequency-swept excitation in pulsed EPR spectroscopy, J. Magn. Reson. (2017).
[118] T. Prisner, Perspectives of shaped pulses for EPR spectroscopy, J. Magn. Reson. (2017).